

Synthetic Aperture Radar: Fundamentals and Applications

Ken Yoong LEE

Centre for Remote Imaging, Sensing and Processing
National University of Singapore

Introduction

□ Aim

- to provide a comprehensive overview of basics and advances in synthetic aperture radar

□ Objectives

- to learn basic principles of SAR data acquisition
- to understand SAR image interpretation
- to gain exposure to a range of SAR applications
- to be aware of freely available SAR data sources and processing software as well as upcoming SAR missions

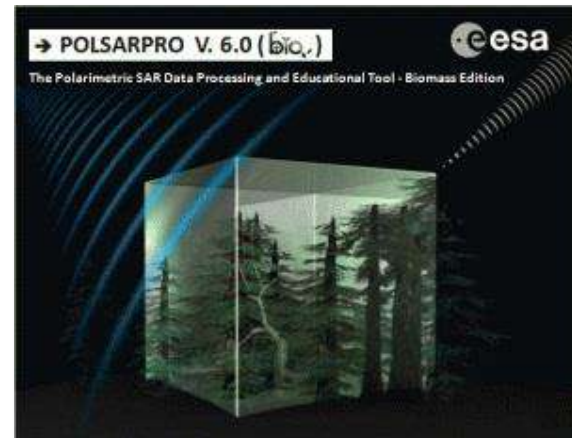
□ Freely available processing software

• **ESA SNAP**

<https://step.esa.int/main/download/snap-download/>

• **PoSARPro**

<https://step.esa.int/main/download/polsarpro-v6-0-biomass-edition-toolbox-download/>



Electromagnetic Waves

- EM waves are disturbances in electric and magnetic fields which are **mutually perpendicular** (oscillating at 90° to each other) and are **in phase**
 - EM waves are produced when an electric charge undergoes acceleration

- EM waves are **transverse waves**
 - an EM wave does not need a medium for propagation



J. C. Maxwell

H. R. Hertz

- Electromagnetic **wave equations** are given by

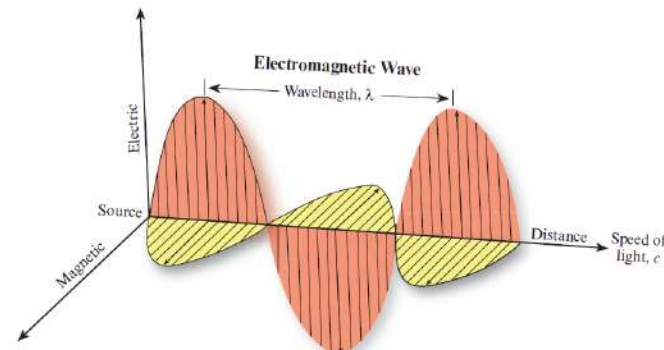
Electric field: $E = E_0 \cos(kx - \omega t)$

Magnetic field: $B = B_0 \cos(kx - \omega t)$

E_0 and B_0 are amplitudes of electric and magnetic fields

x and t refer to distance and time, respectively

k and ω denote separately angular wave number and angular frequency



Electromagnetic Waves

- EM waves can travel through vacuum at the speed of $299\ 792\ 458\ \text{m s}^{-1}$
→ the speed of EM waves in vacuum is a fundamental constant and same for all frequencies
- Wave velocity equation is applicable to all electromagnetic waves

$$v = f\lambda = \omega / k$$

v represents velocity of an electromagnetic wave

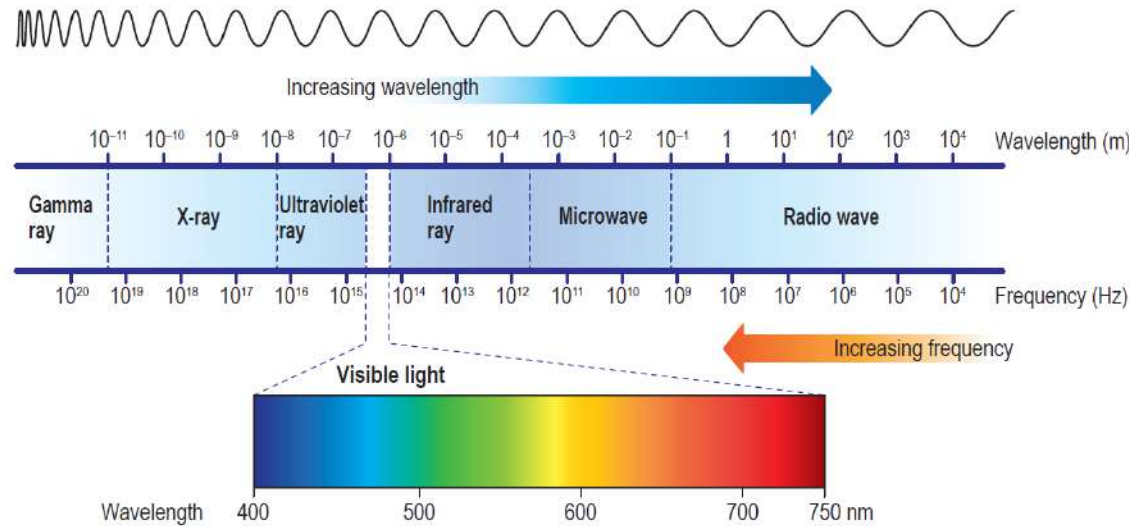
f and λ are refer to frequency and wavelength of an electromagnetic wave

$$\omega = 2\pi f \text{ and } k = 2\pi / \lambda$$

- When EM waves travel from one medium to another ,
 - frequencies remain unchanged, which depends only on the source of the wave
 - speeds and wavelengths do change
- EM waves obey the laws of reflection and refraction

Electromagnetic Waves

- EM waves are classified based on their frequencies in **electromagnetic spectrum**



- EM waves **transfer energy** from one place to another
- EM waves **carry no electric charge** as they are neither positively nor negatively charged

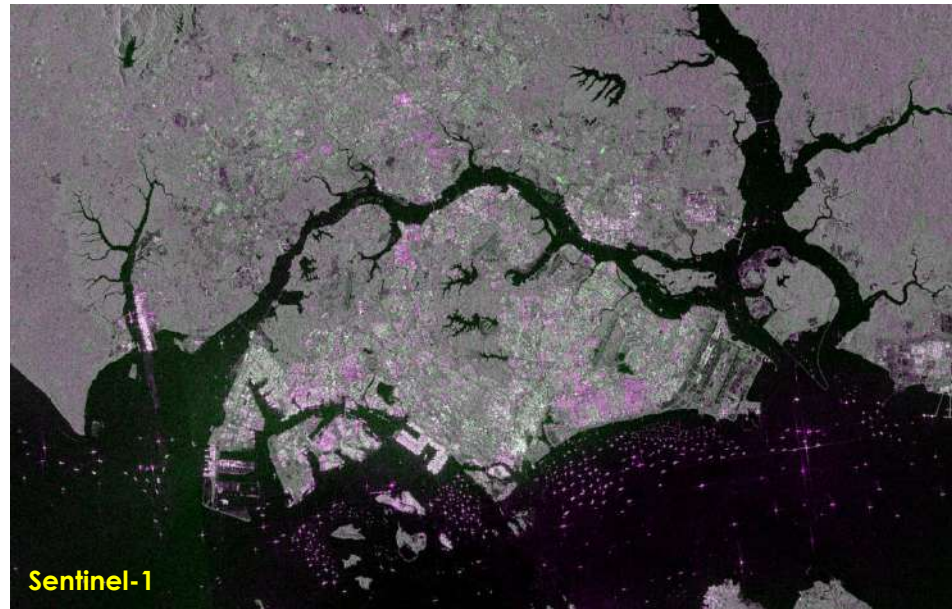
Electro-Optical Versus Synthetic Aperture Radar

- **optical and microwave** spaceborne remotely sensed data are **complementary**



electro-optical data

- passive system, which relies on sunlight
- data acquisition cannot see through clouds
- optical images are easier to be interpreted

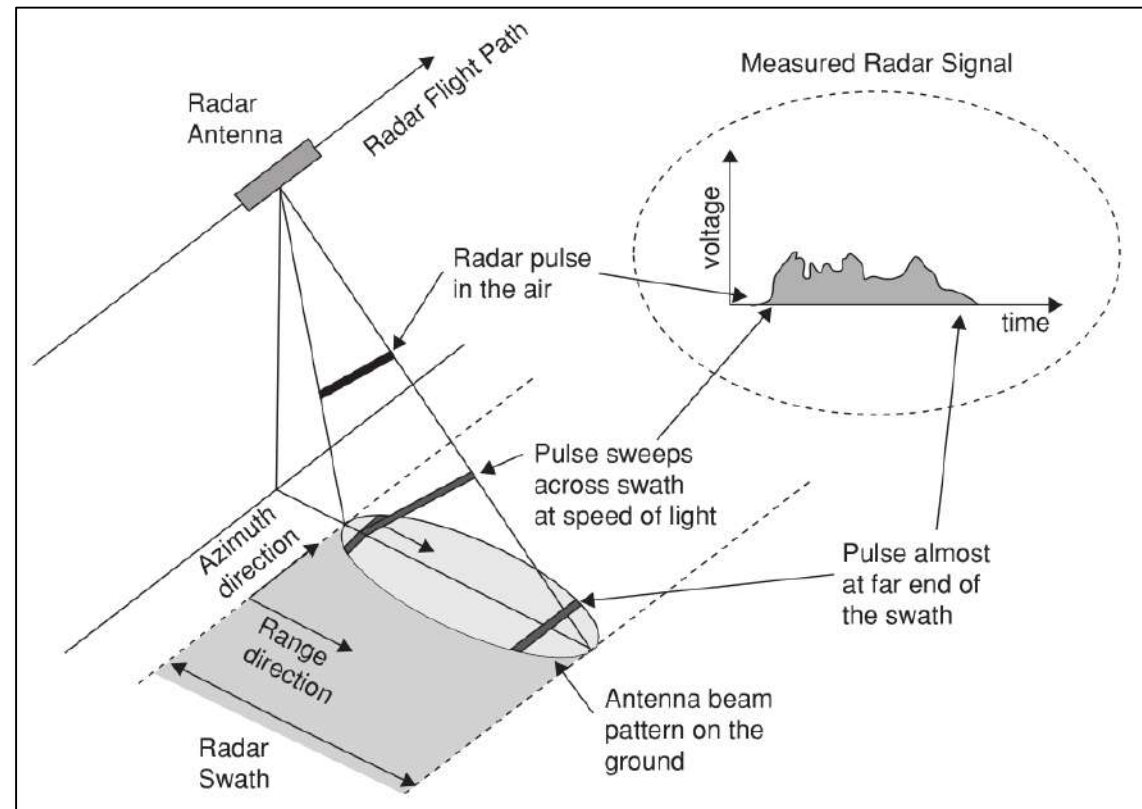
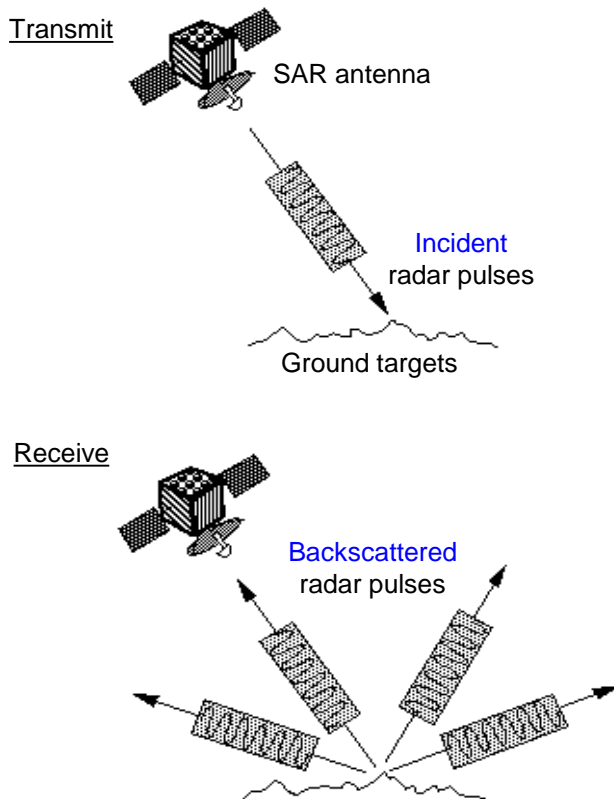


synthetic aperture radar data

- **active** system, which works in all weather and day/night
- speckle influence and geometric distortions
- SAR image interpretation is not straightforward

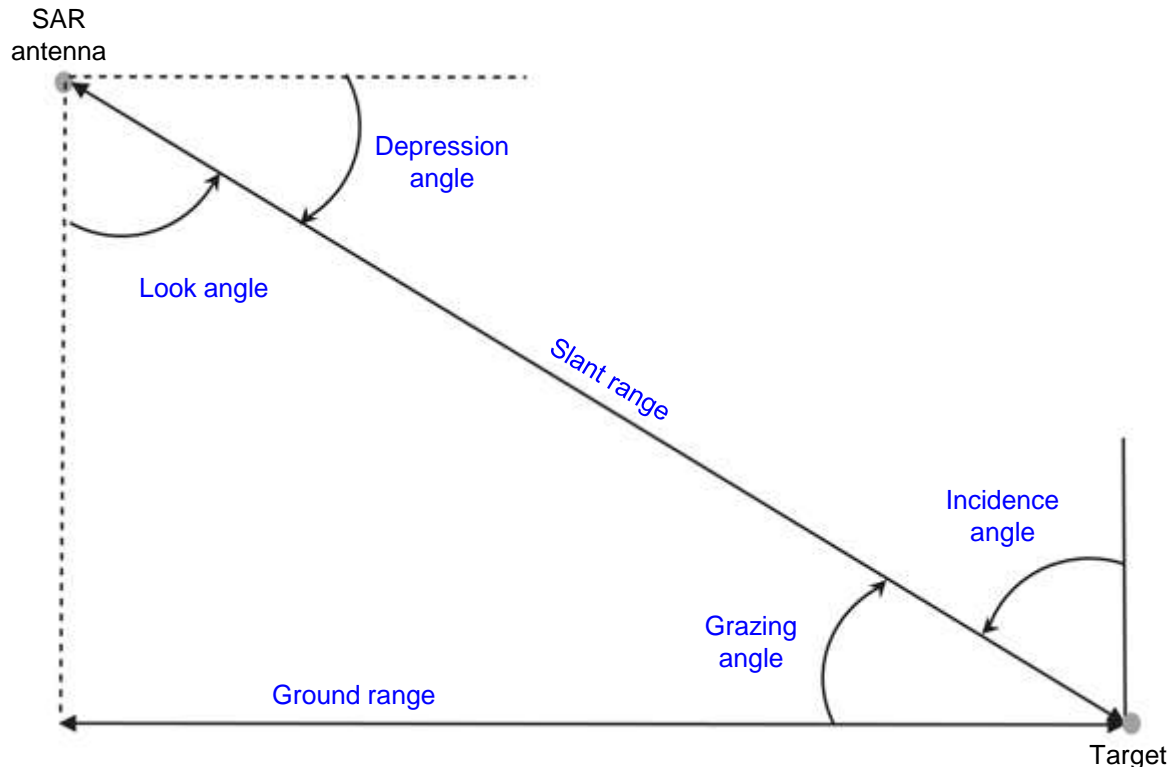
Radar Fundamentals

- Acronym for Radio Detection And Ranging

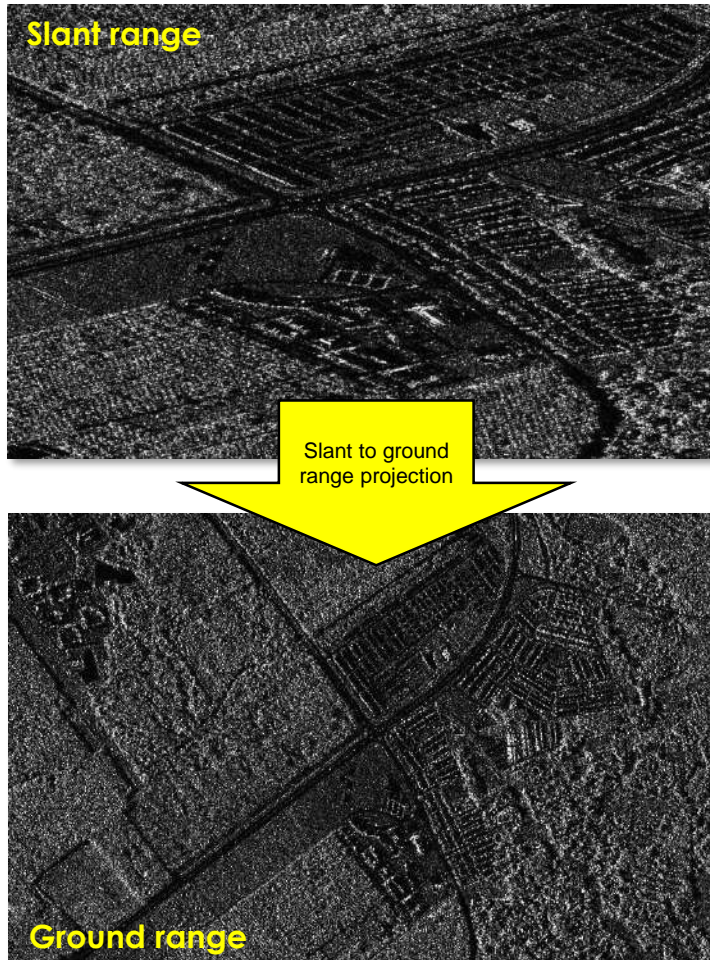


Imaging Geometry

- **Side-look imaging**

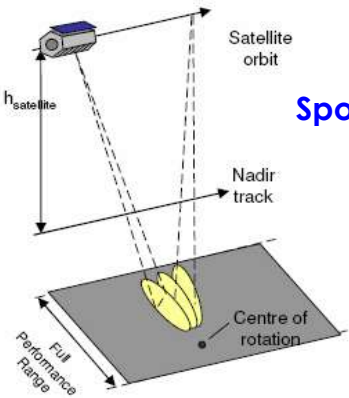


Target → deterministic/discrete object or distributed surface

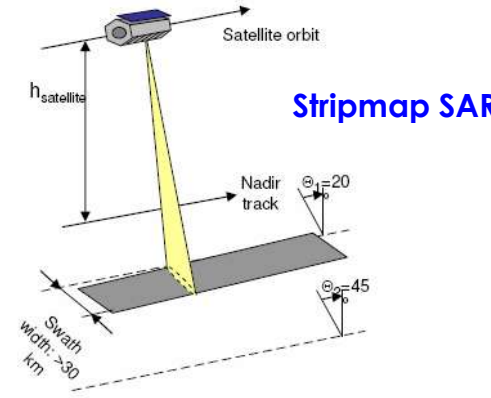


Radar Imaging

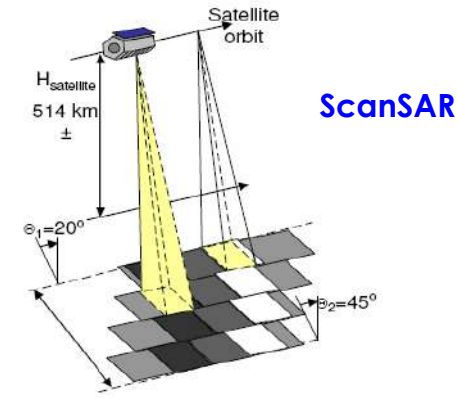
□ Acquisition modes



Spotlight SAR

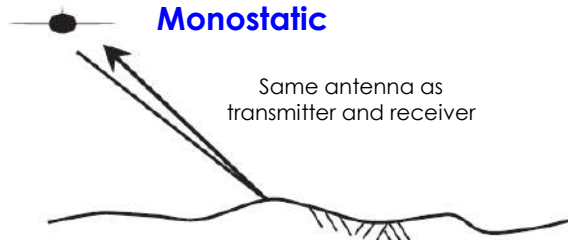


Stripmap SAR

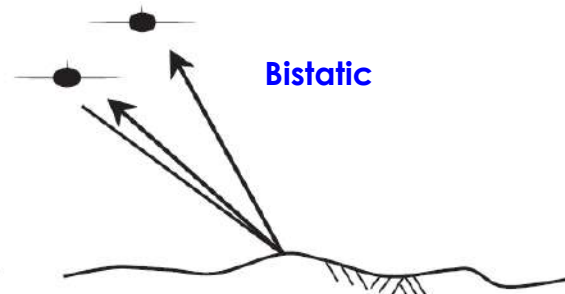


ScanSAR

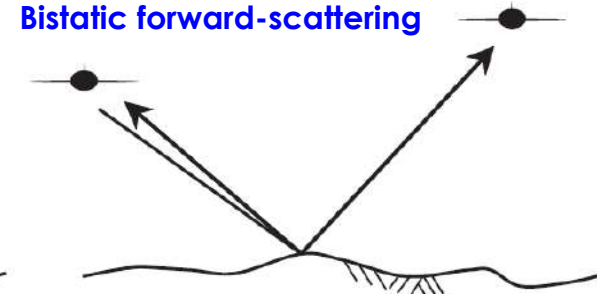
□ Operating configurations



Monostatic



Bistatic



Bistatic forward-scattering

Radar Band Designation and Polarisation

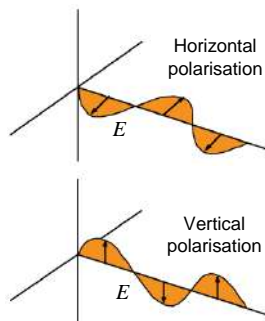
□ Radar bands :

Band	Frequency	Wavelength
P	0.3 - 1 GHz	30 - 100 cm
L	1 - 2 GHz	15 - 30 cm
S	2 - 4 GHz	7.5 - 15 cm
C	4 - 8 GHz	3.8 - 7.5 cm
X	8 - 12.5 GHz	2.4 - 3.8 cm
Ku	12.5 - 18 GHz	1.7 - 2.4 cm
K	18 - 26.5 GHz	1.1 - 1.7 cm
Ka	26.5 - 40 GHz	0.75 - 1.1 cm



□ Polarisation :

Locus of the tip of the electric field vector of electromagnetic wave observed in a plane orthogonal to the wave normal (IEEE, 1997)



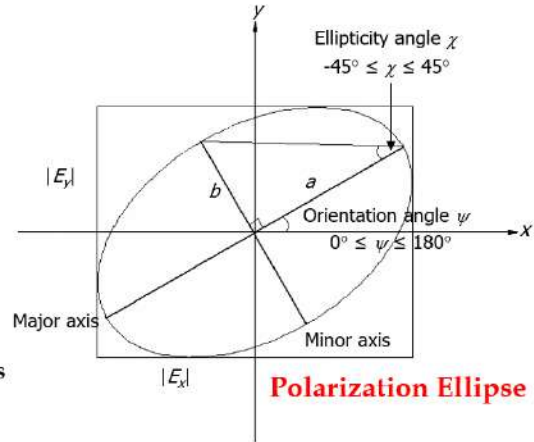
Polarization State (IEEE, 1993)

At a given point, the **condition** of the polarization of a plane wave as described by **axial ratio**, **orientation angle**, and **polarization sense**

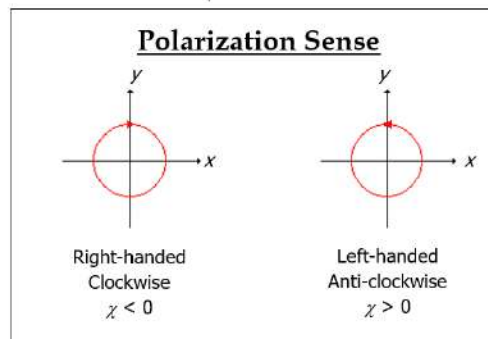
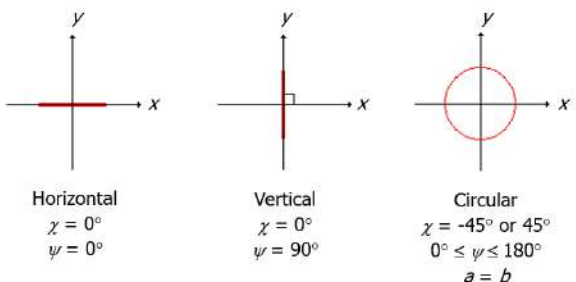
$$\text{Axial ratio : } r = \frac{b}{a}$$

$$\text{Ellipticity angle : } \chi = \tan^{-1} \frac{b}{a}$$

Orientation angle : angle between major axis and reference axis



Polarization Sense



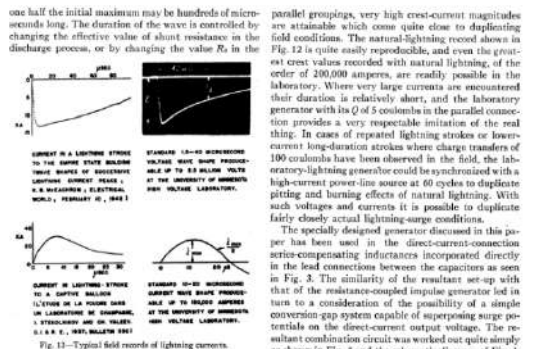
IEEE (1993). IEEE Standard Definitions of Terms for Antennas. IEEE: New York, p. 33.

Friis Transmission Equation



Harald T. Friis
(22 February 1893 – 15 June 1976)

https://en.wikipedia.org/wiki/Harald_T._Friis



generally used impulse generator connection shown in Fig. 11(a). The equivalent circuit diagrams as given in the lower part of Fig. 11 have been proved a rather good approximation of the distributed network allowing fairly accurate calculation of the output wave shapes produced.

A comparison of typical laboratory wave shapes with similar field records of lightning strokes is given in Fig. 12. By reconnecting the capacitors of the generator in

HAROLD T. FRIIS†, FELLOW, I.R.E.

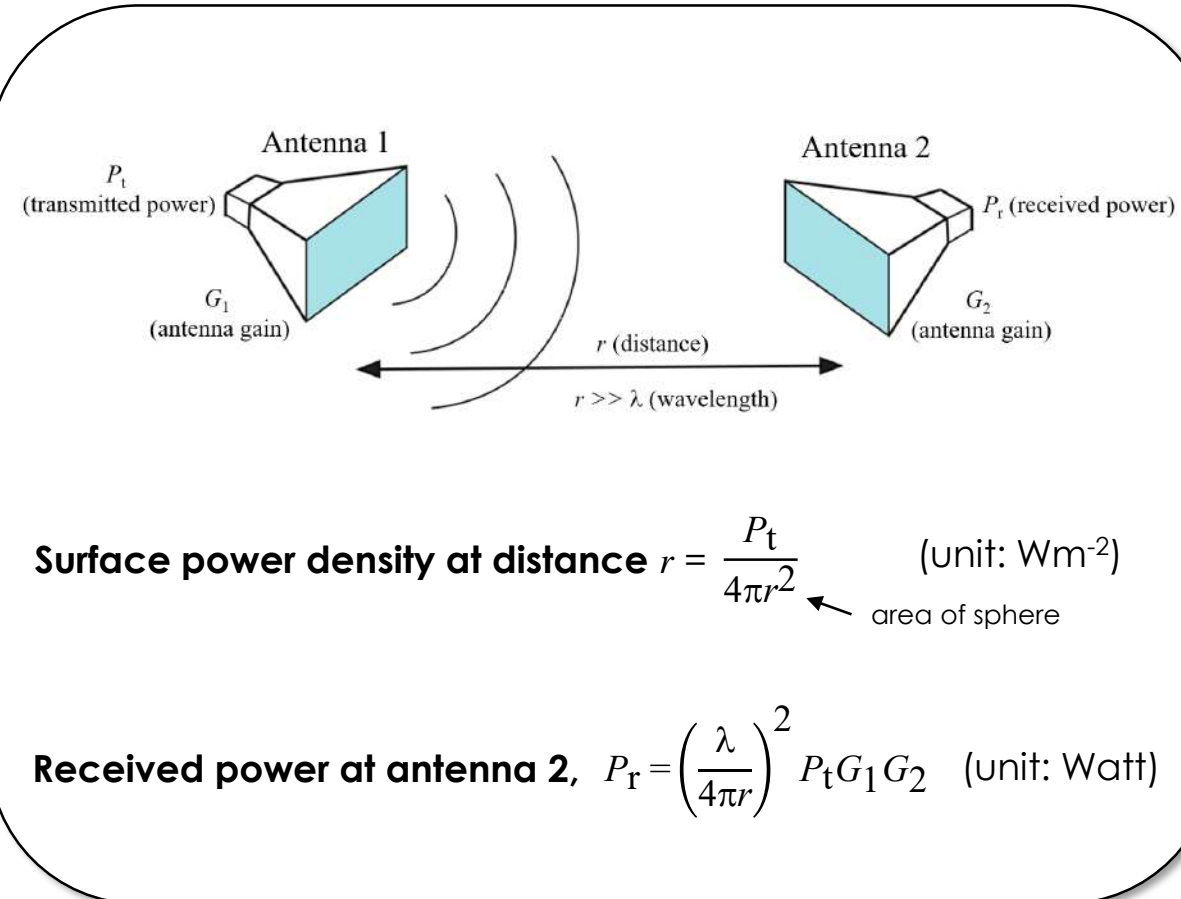
Summary—A simple transmission formula for a radio circuit is derived. The utility of the formula is emphasized and its limitations are discussed.

INTRODUCTION

THIS NOTE emphasizes the utility of the following simple transmission formula for a radio circuit made up of a transmitting antenna and a receiving antenna in free space:

$$\frac{P_r}{P_t} = \frac{A_r A_t}{d^2} \quad (1)$$

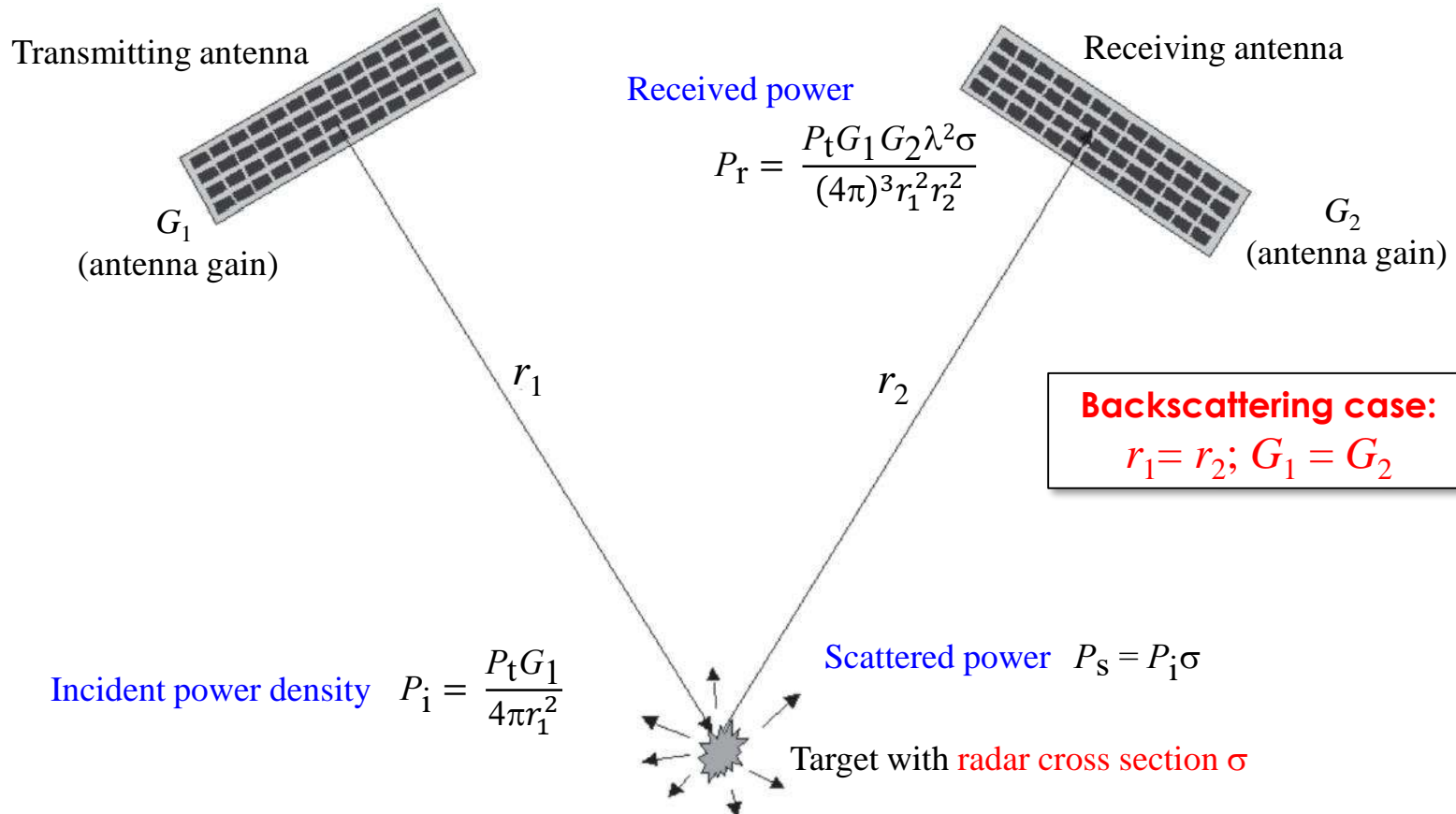
where
• Design classification: R120. Original manuscript received by the Institution, December 6, 1945.
• Bell Telephone Laboratories, Holmdel, N. J.



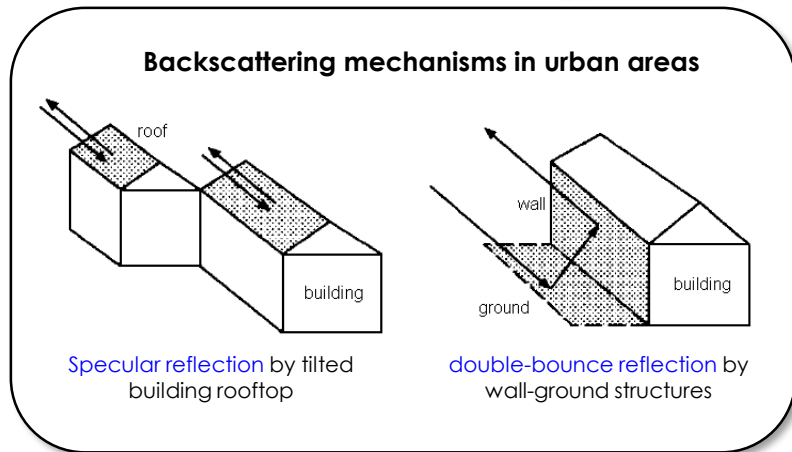
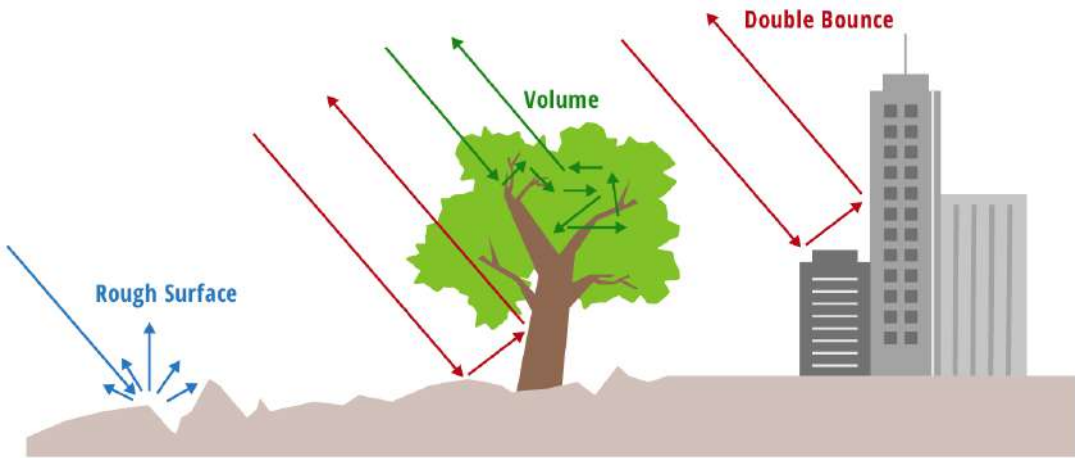
Surface power density at distance $r = \frac{P_t}{4\pi r^2}$ (unit: Wm^{-2})

Received power at antenna 2, $P_r = \left(\frac{\lambda}{4\pi r}\right)^2 P_t G_1 G_2$ (unit: Watt)

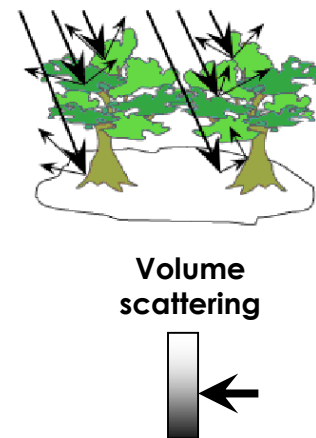
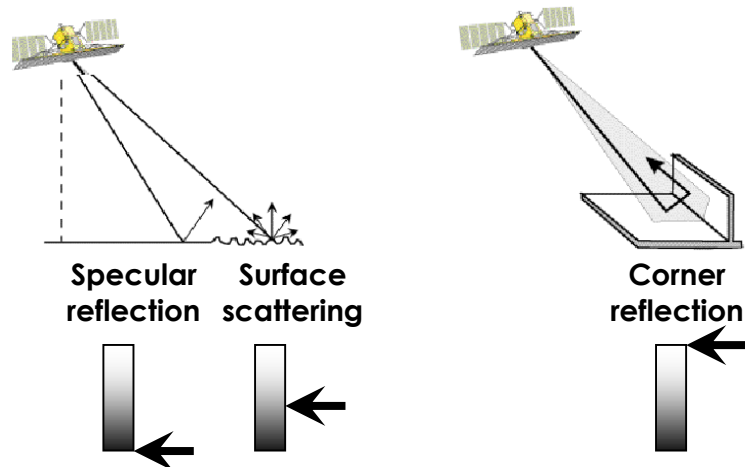
Radar Range Equation



Wave-Matter Interactions



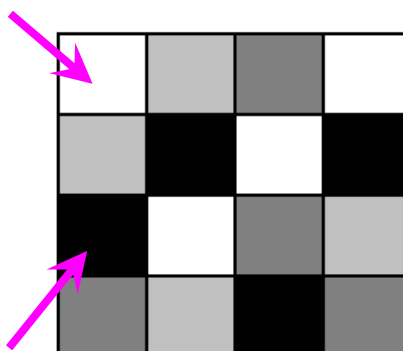
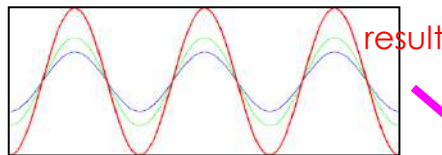
Brightness appearance
in SAR image



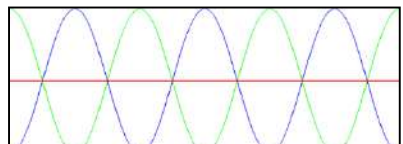
SAR Image Speckle

- Arises from **random interference of backscattered radar waves** from elementary scatterers within an illuminated resolution cell
- SAR image appears **grainy** due to the presence of speckles

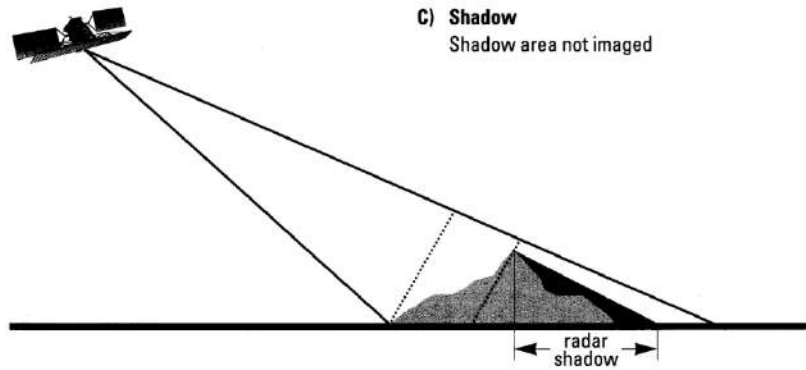
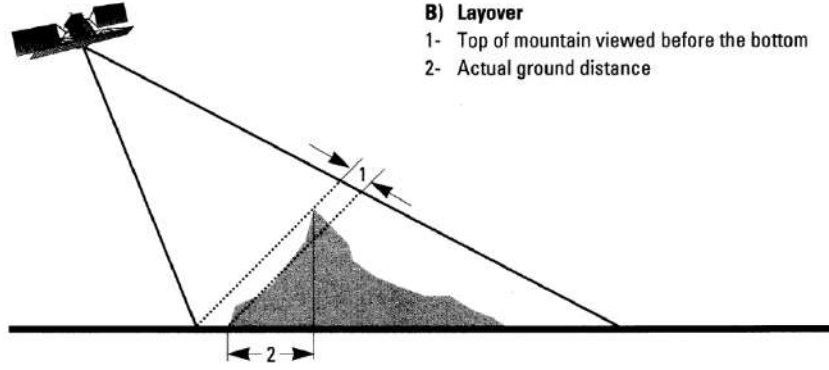
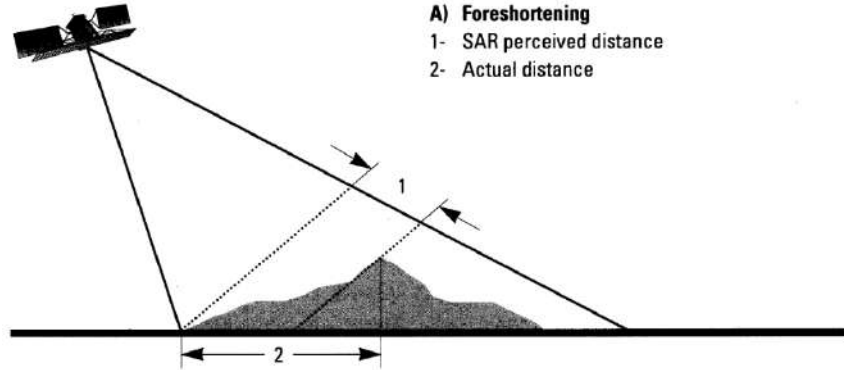
Constructive interference
(in phase)



Destructive interference
(out of phase)

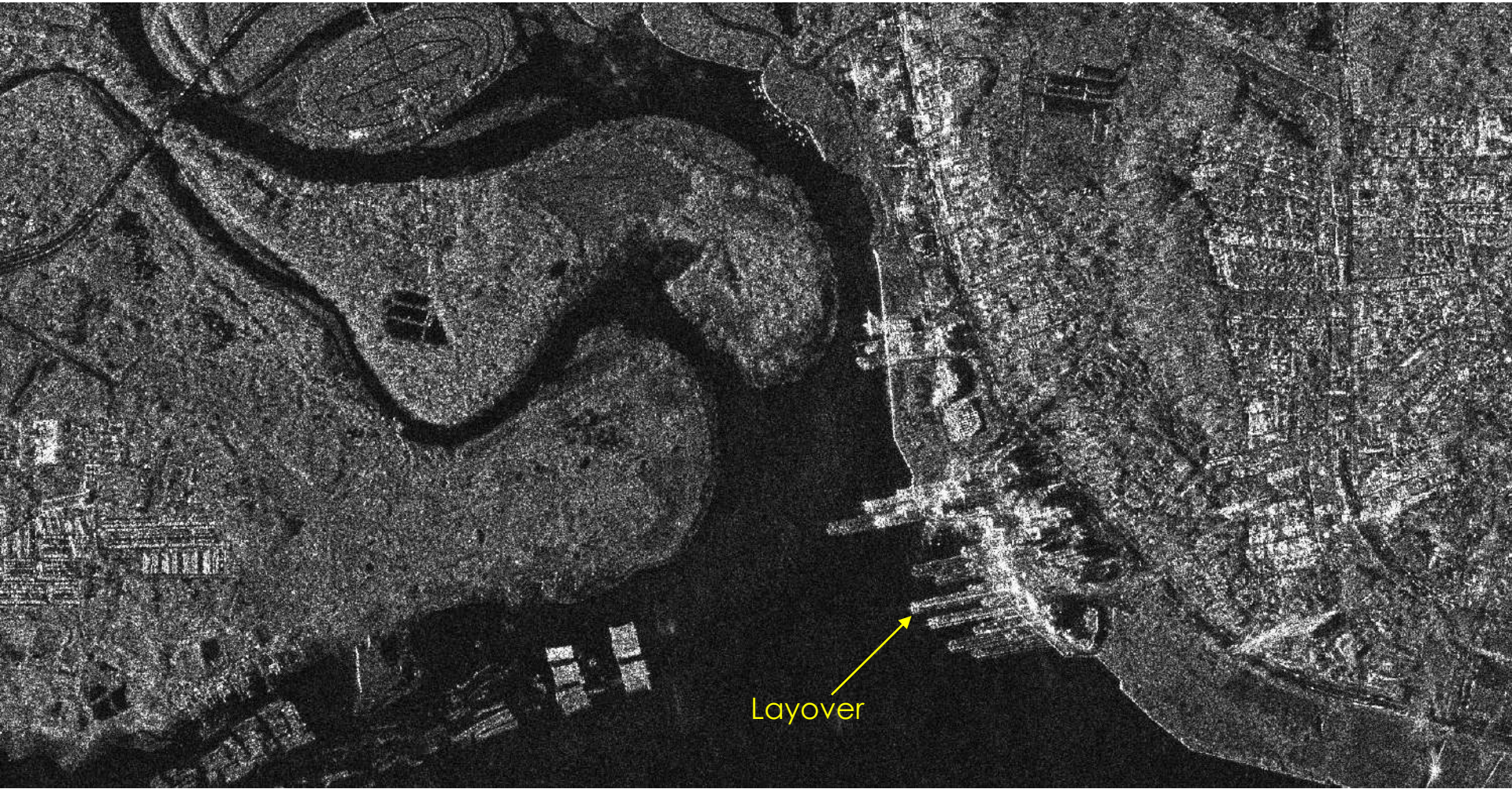


Geometric Distortions in SAR Image

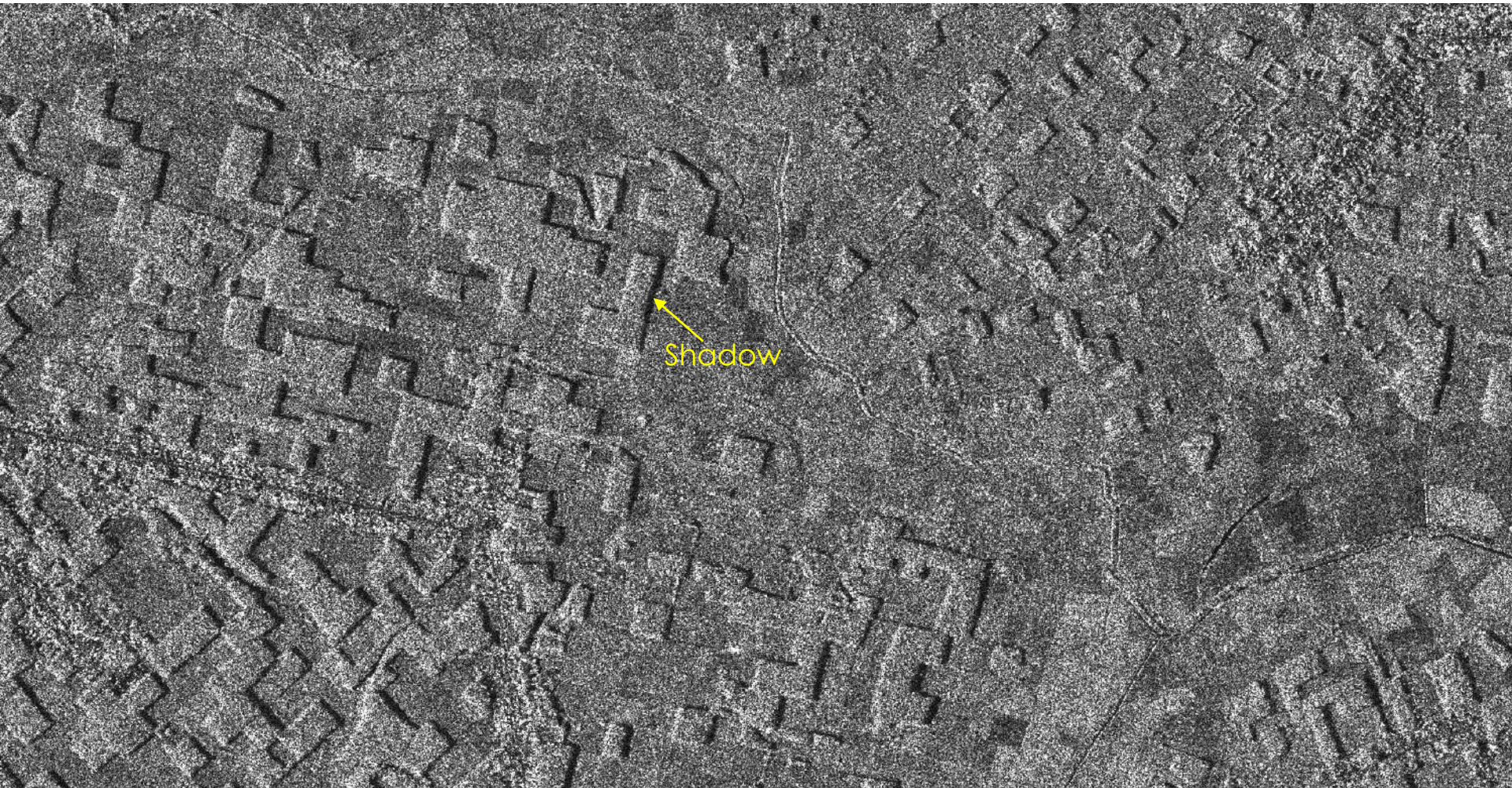


SPOT 6 (acquired on 30th Jan 2022)





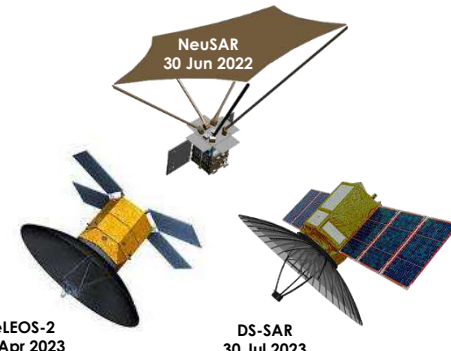
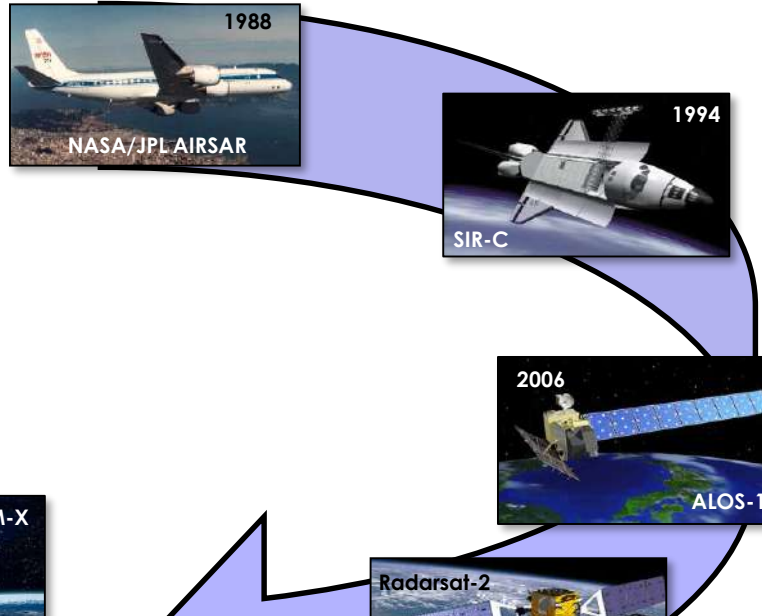
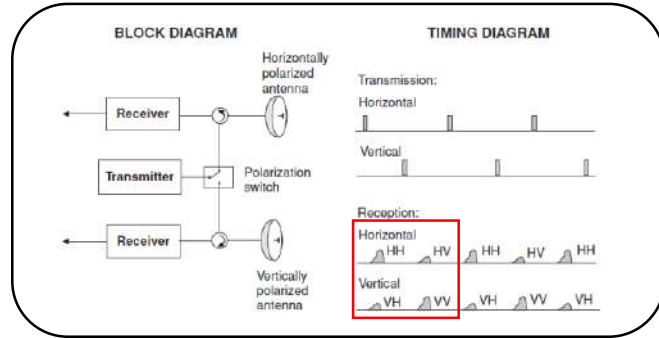
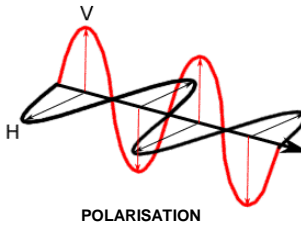




Radar Polarimetry

Radar Polarimetry

- ❑ Polarimetric radar **transmits alternatively pulses out of horizontally and vertically polarised antennas and receives at both polarisations simultaneously** (van Zyl and Kim, 2011)
- ❑ **2 pulses** are needed to measure the **full scattering matrix** of an illuminated target



Radar Polarimetry

Scattering matrix

$$S = \begin{bmatrix} S_{HH} & S_{HV} \\ S_{VH} & S_{VV} \end{bmatrix}$$

Kennaugh
matrix

Covariance
matrix

Coherency
matrix

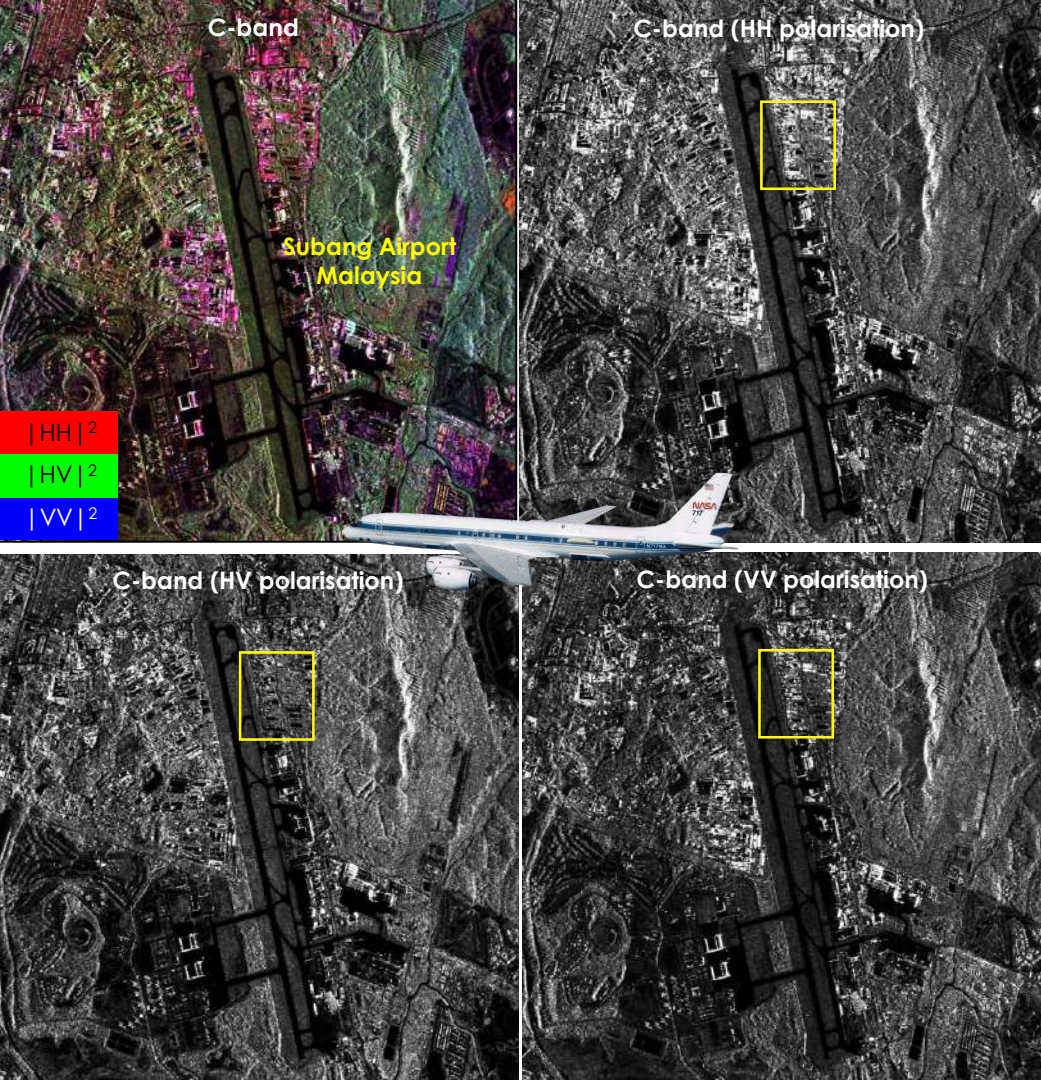
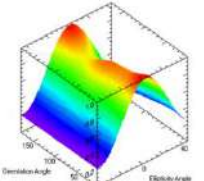
Incoherence components

- Intensity, total power, polarisation ratio

Coherence components

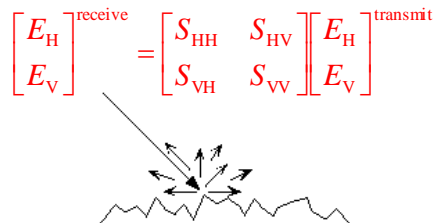
- Coherence coefficient, phase difference

Polarisation signatures



Scattering Matrix

- **2×2 complex matrix (also called Sinclair matrix)**
- **symmetric matrix (in backscatter alignment) where $S_{\text{HV}} = S_{\text{VH}}$ (for reciprocal target)**

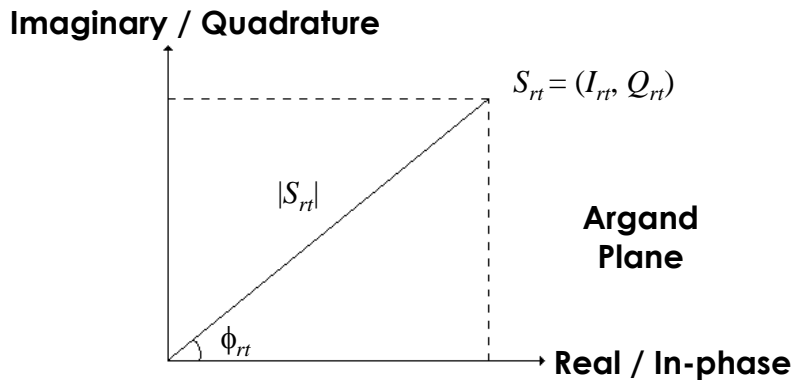


$$S = \begin{bmatrix} S_{\text{HH}} & S_{\text{HV}} \\ S_{\text{VH}} & S_{\text{VV}} \end{bmatrix} = \begin{bmatrix} A_{\text{HH}} e^{j\phi_{\text{HH}}} & A_{\text{HV}} e^{j\phi_{\text{HV}}} \\ A_{\text{VH}} e^{j\phi_{\text{VH}}} & A_{\text{VV}} e^{j\phi_{\text{VV}}} \end{bmatrix} = \begin{bmatrix} I_{\text{HH}} + jQ_{\text{HH}} & I_{\text{HV}} + jQ_{\text{HV}} \\ I_{\text{VH}} + jQ_{\text{VH}} & I_{\text{VV}} + jQ_{\text{VV}} \end{bmatrix}$$

Amplitude : $A_{rt} = |S_{rt}| = \sqrt{I_{rt}^2 + Q_{rt}^2}$

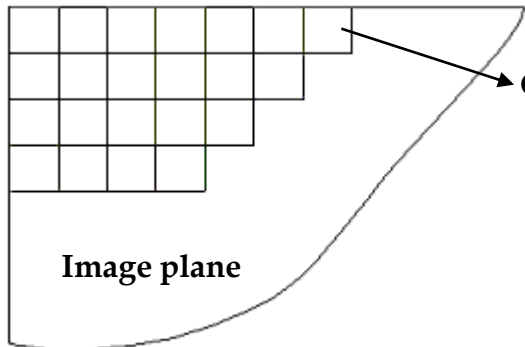
Intensity : $P_{rt} = |S_{rt}|^2 = S_{rt} S_{rt}^* = A_{rt}^2 = I_{rt}^2 + Q_{rt}^2$

Phase : $\phi_{rt} = \tan^{-1} \frac{Q_{rt}}{I_{rt}}$



Matrix Representations in Multilook PolSAR Data

□ Covariance matrix : $\mathbf{C} = \mathbf{C}^{*T}$ (Hermitian matrix)



$$\mathbf{C} = \langle \mathbf{s} \mathbf{s}^{*T} \rangle = \begin{bmatrix} \langle s_{HH} \rangle \\ \langle \sqrt{2} s_{HV} \rangle \\ \langle s_{VV} \rangle \end{bmatrix} \begin{bmatrix} \langle s_{HH}^* \rangle & \langle \sqrt{2} s_{HV}^* \rangle & \langle s_{VV}^* \rangle \end{bmatrix}$$

* and T denote the complex conjugate and transpose
 $\langle \cdot \rangle$ is the ensemble average

$$\begin{bmatrix} c_{11} & c_{12} & c_{13} \\ c_{12}^* & c_{22} & c_{23} \\ c_{13}^* & c_{23}^* & c_{33} \end{bmatrix} = \begin{bmatrix} \langle |s_{HH}|^2 \rangle & \langle \sqrt{2} s_{HH} s_{HV}^* \rangle & \langle s_{HH} s_{VV}^* \rangle \\ \langle \sqrt{2} s_{HV}^* s_{HH} \rangle & \langle 2|s_{HV}|^2 \rangle & \langle \sqrt{2} s_{HV} s_{VV}^* \rangle \\ \langle s_{HH}^* s_{VV} \rangle & \langle \sqrt{2} s_{HV}^* s_{VV} \rangle & \langle |s_{VV}|^2 \rangle \end{bmatrix}$$

- Diagonal elements (variances) are **intensity** components
- Off-diagonal elements (covariances) contain phase difference information
- Total power (or span) is sum of diagonal elements
- Determinant of covariance matrix is known as **generalised variance**

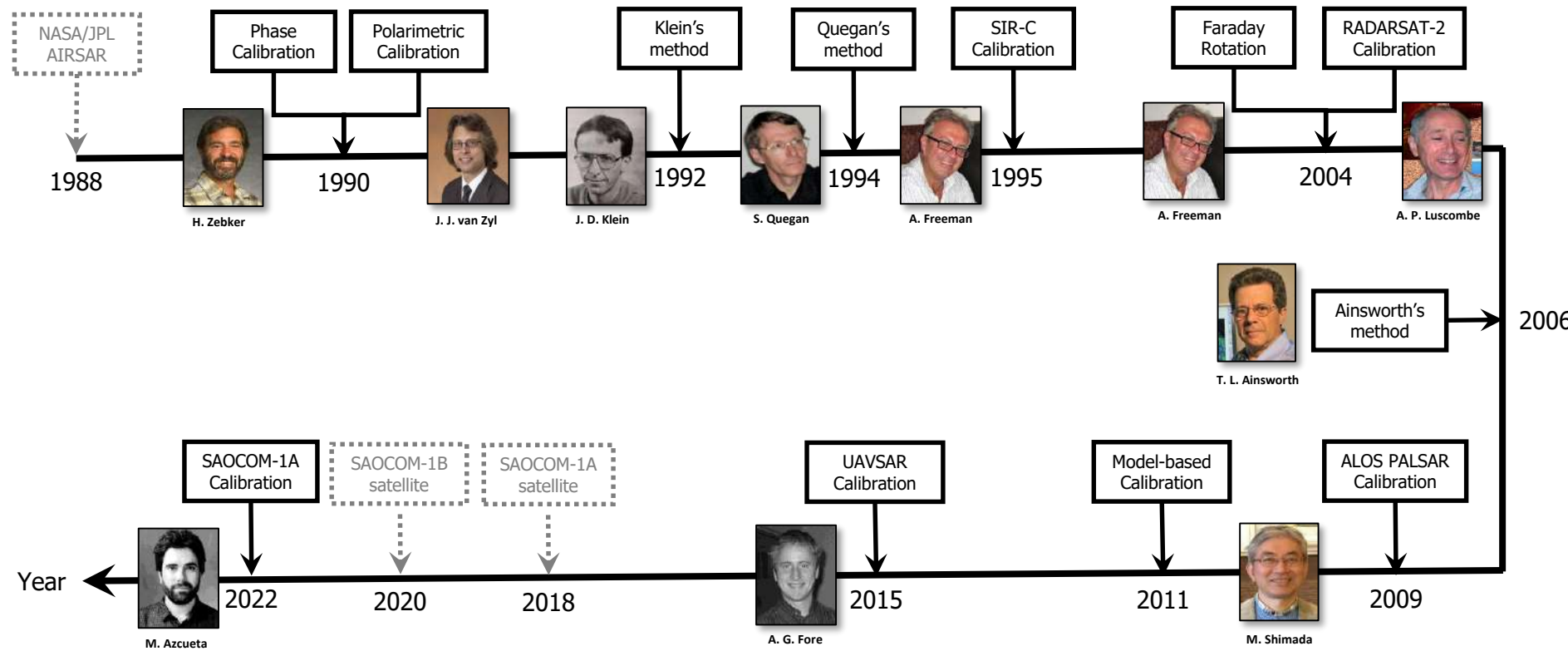
□ Coherency matrix : $\mathbf{T} = \mathbf{N} \mathbf{C} \mathbf{N}^T$

$$\mathbf{T} = \frac{1}{2} \left\{ \begin{bmatrix} |s_{HH} + s_{VV}|^2 & (s_{HH} + s_{VV})(s_{HH} - s_{VV})^* & 2(s_{HH} + s_{VV})s_{HV}^* \\ (s_{HH} - s_{VV})(s_{HH} + s_{VV})^* & |s_{HH} - s_{VV}|^2 & 2(s_{HH} - s_{VV})s_{HV}^* \\ 2s_{HV}(s_{HH} + s_{VV})^* & 2s_{HV}(s_{HH} - s_{VV})^* & 4|s_{HV}|^2 \end{bmatrix} \right\} \text{ where } \mathbf{N} = \frac{1}{\sqrt{2}} \begin{bmatrix} 1 & 0 & 1 \\ 1 & 0 & -1 \\ 0 & \sqrt{2} & 0 \end{bmatrix}$$

Polarimetric Calibration

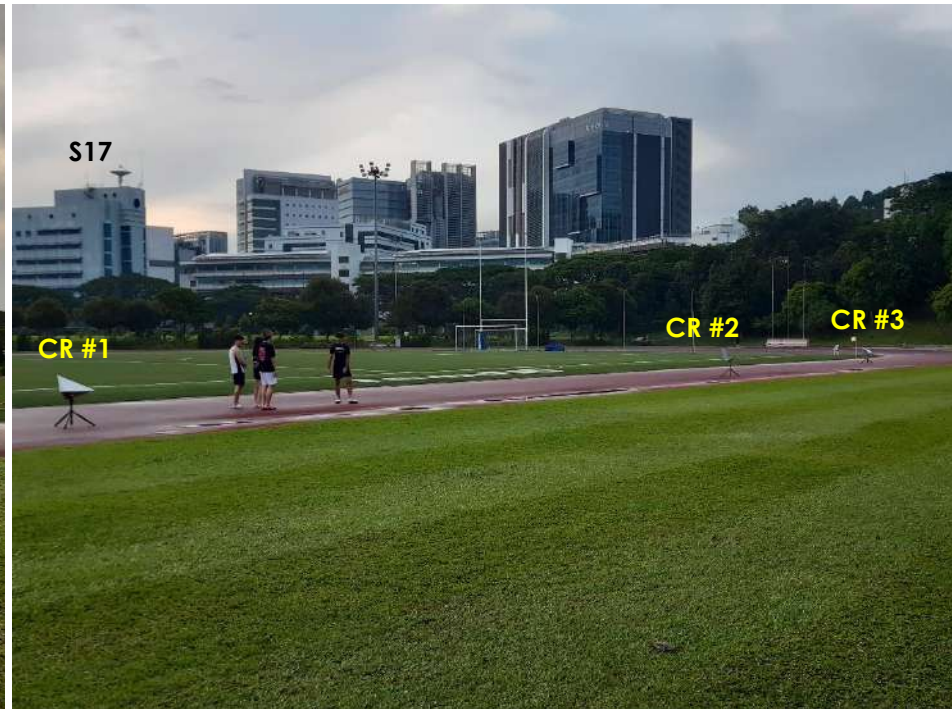
Polarimetric Calibration

- PolSAR imaging systems are **imperfect** in reality
- Relative phase, channel imbalance, and crosstalk are required to be compensated



Corner Reflectors for Polarimetric Calibration

- 2 trihedral and 1 dihedral corner reflectors (CRs) were deployed near NUS football field
- Trihedral and dihedral CRs have their edge length of 50 cm
- Dihedral CR was tilted up about 17°, while trihedral CRs were about 27°
- There was heavy rain around 2 a.m. As expected, the running track was still wet

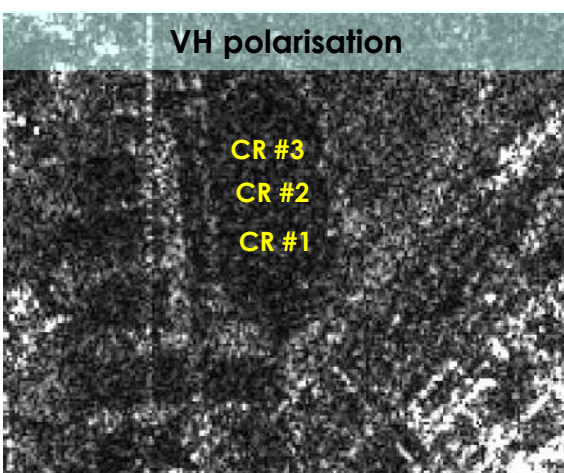
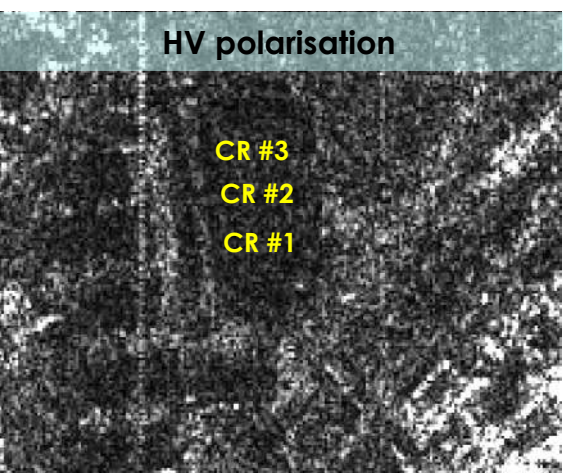
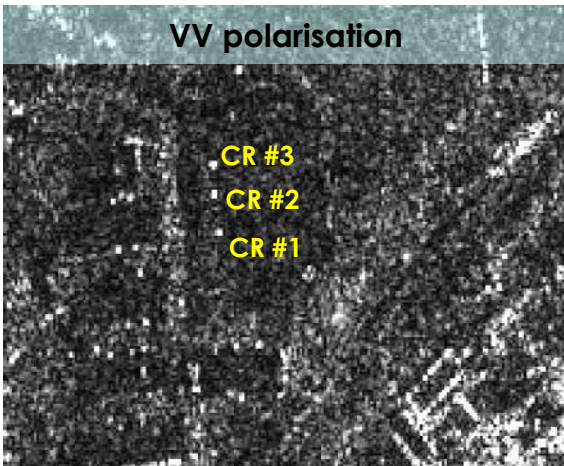
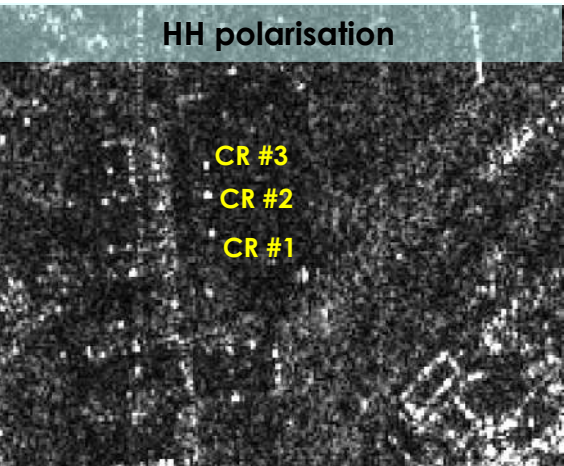
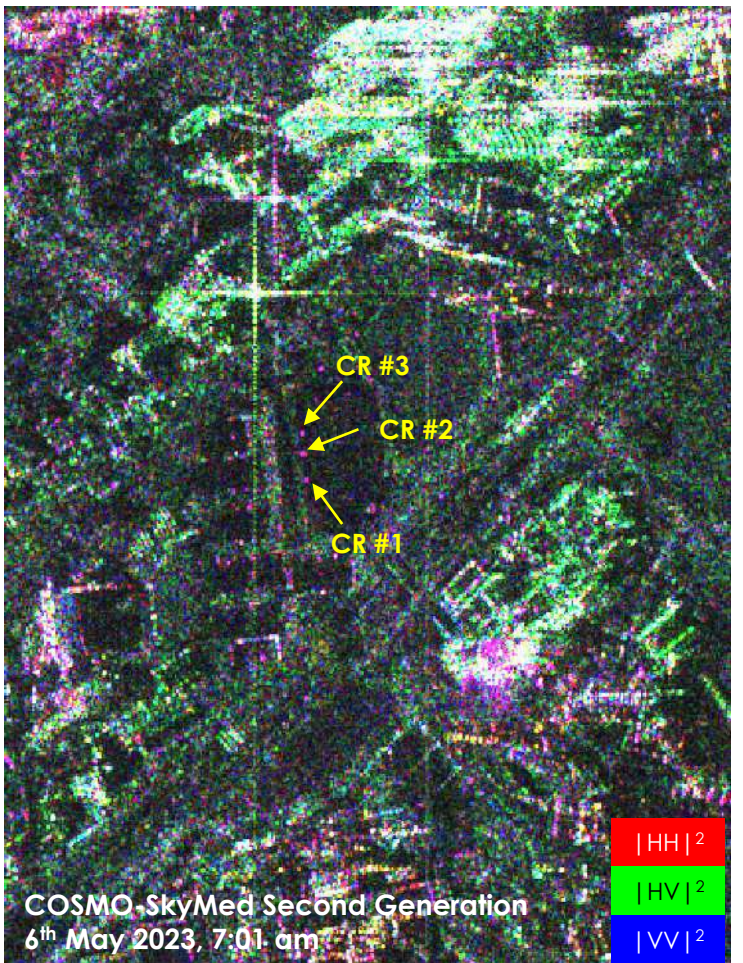


Corner Reflectors for Polarimetric Calibration

- Trihedral CR is **rotation-invariant**, but it is not the case for dihedral CR. Hence, a careful and proper setup is always required for the latter. In this experiment, **no rotation** was applied to the dihedral CR (i.e., zero rotation angle)



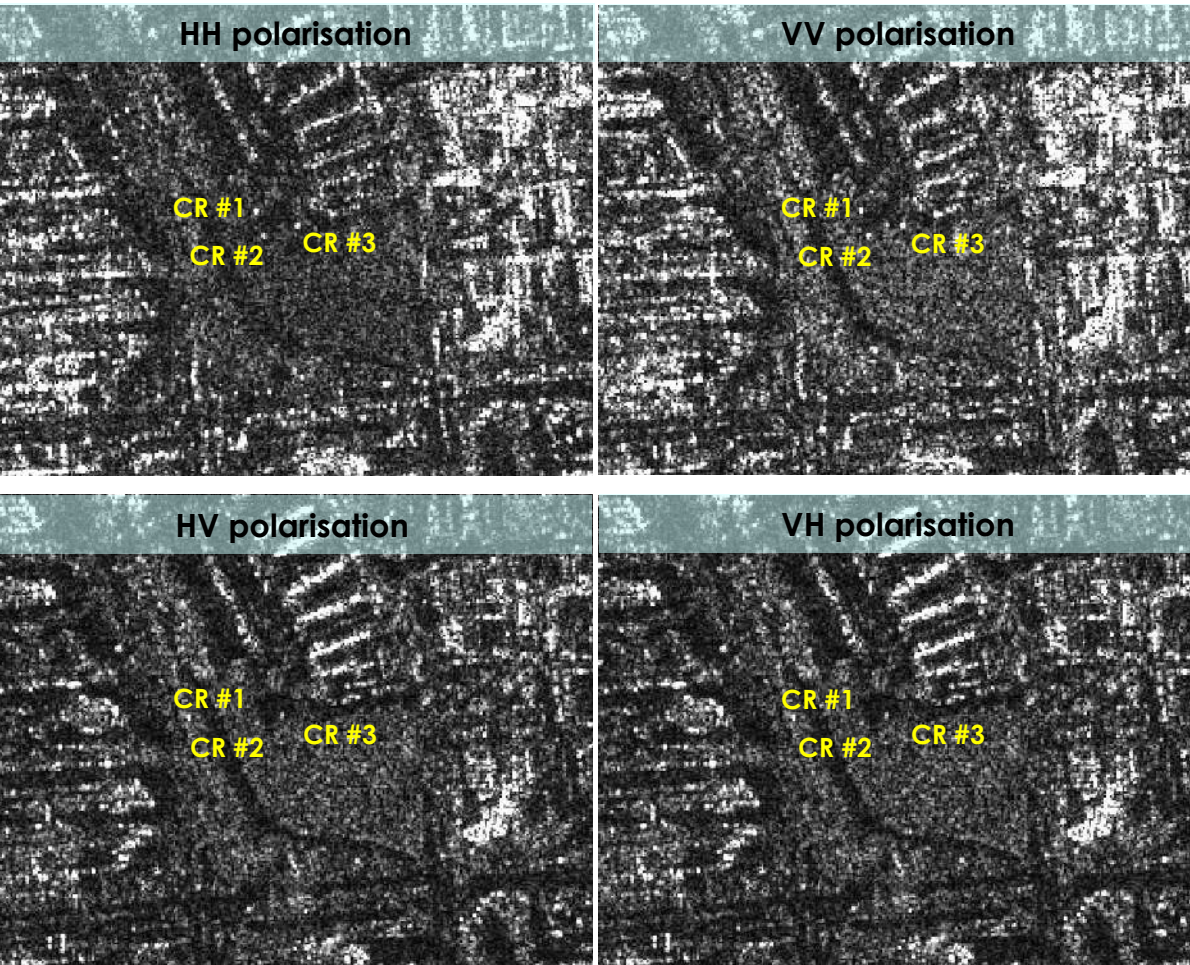
Polarimetric Response of CRs



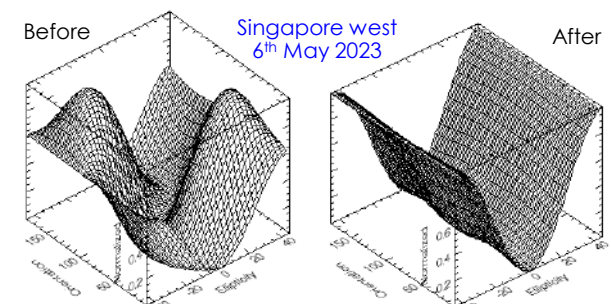
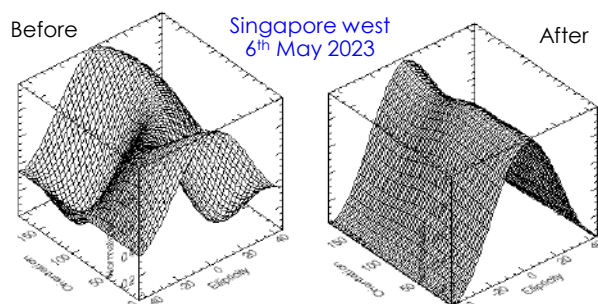
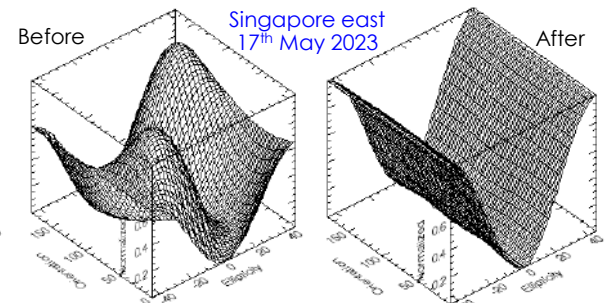
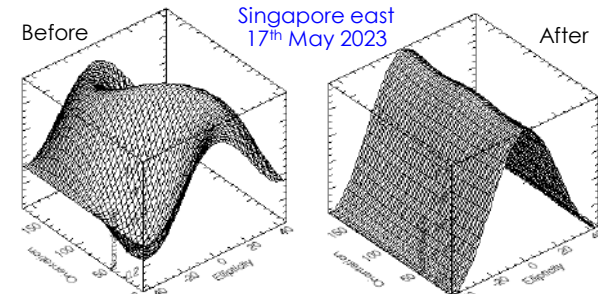
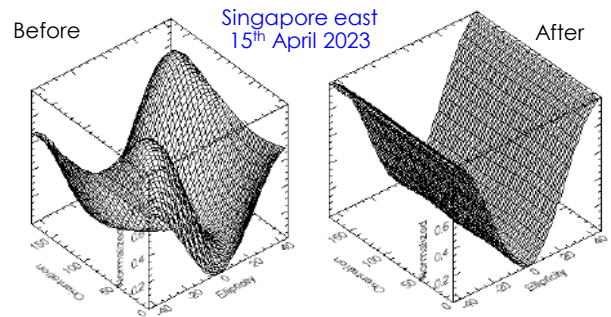
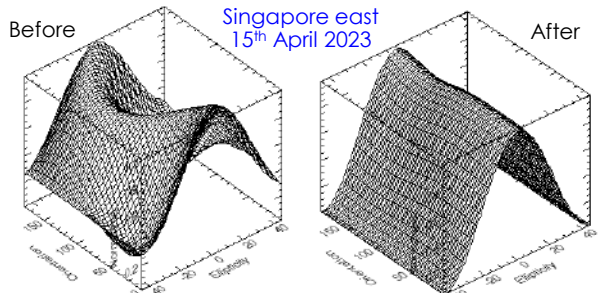
- 2 trihedral and 1 dihedral corner reflectors (CRs) were deployed next to Defu Lane 10
- Trihedral and dihedral CRs have their edge length of 50 cm
- Dihedral CR was tilted up about 4° , while trihedral CRs were about 14°



Polarimetric Response of CRs



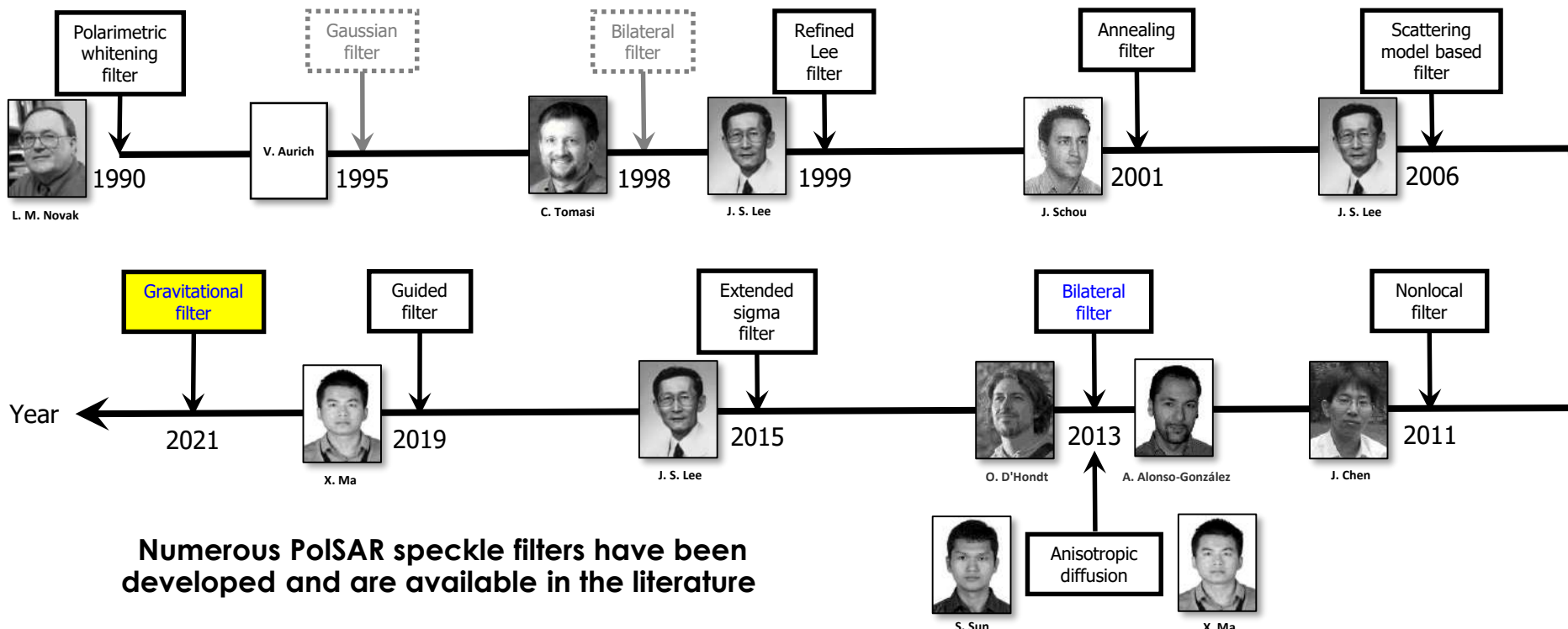
Polarisation Signatures Before and After Calibration



Speckle Filtering

Polarimetric Speckle Filtering

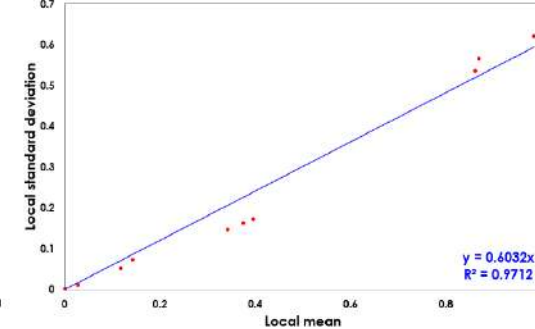
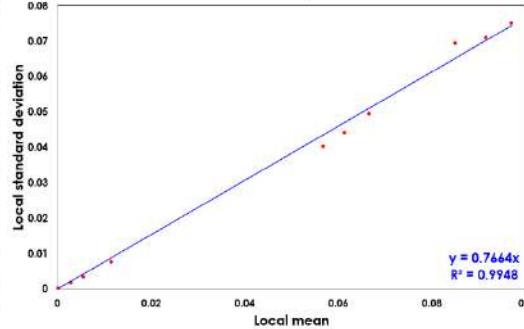
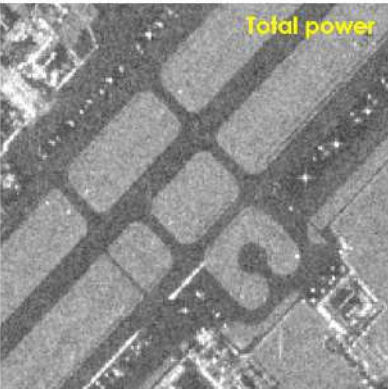
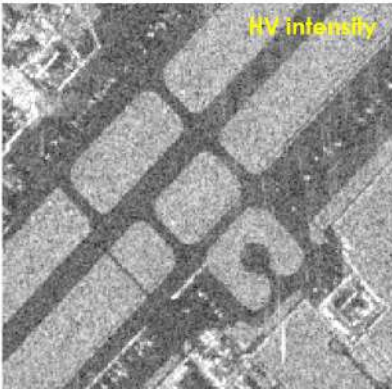
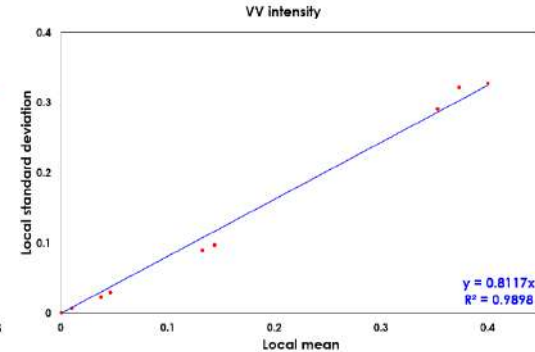
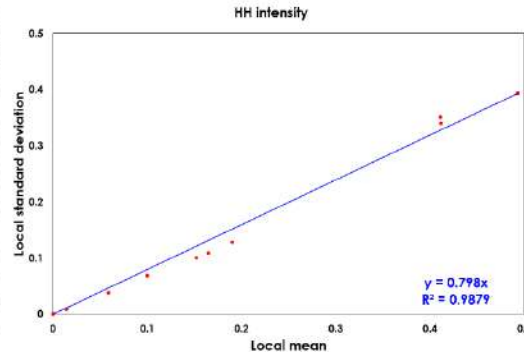
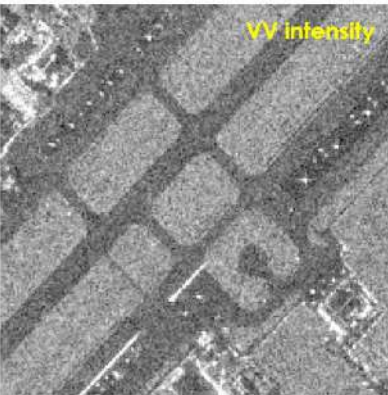
- Speckle appears inherently in SAR images due to constructive and destructive interference of backscattering from many elementary scatterers within an illuminated resolution cell



Speckle Modelling

☐ Multiplicative Noise Model (Lee, 1981)

- Also known as signal-dependent noise → When local mean increases, local standard deviation increases linearly



Unfiltered



Boxcar filter (3×3 window)



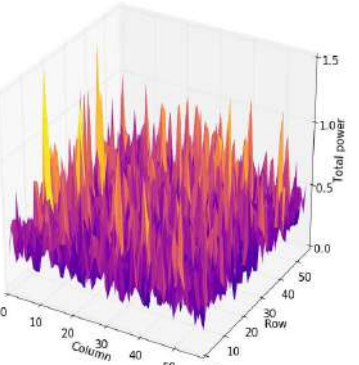
Boxcar filter (7×7 window)



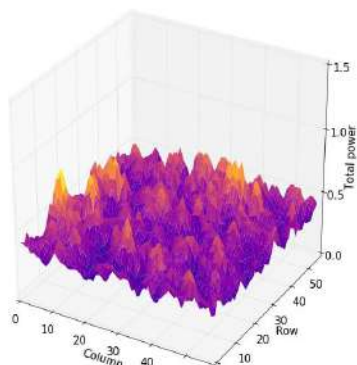




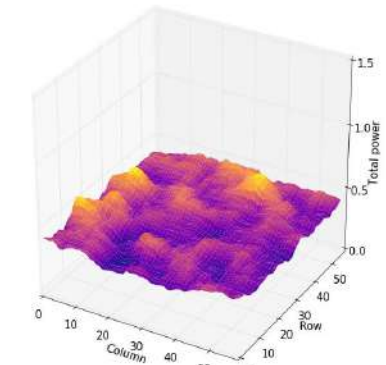
Unfiltered
 $\sigma = 0.1728$



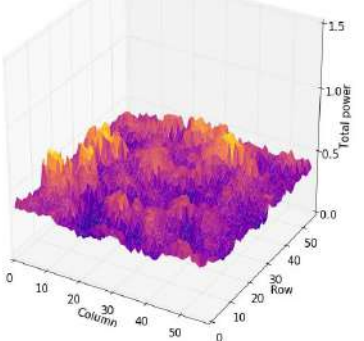
Boxcar filter (3×3 window)
 $\sigma = 0.0780$



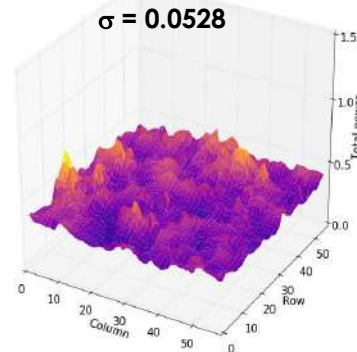
Boxcar filter (7×7 window)
 $\sigma = 0.0441$



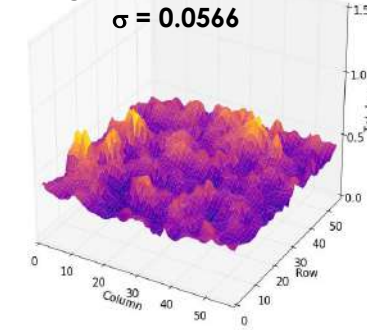
Lee refined filter (7×7 window)
 $\sigma = 0.0594$



Gravitational filter (7×7 window)
full matrix
 $\sigma = 0.0528$



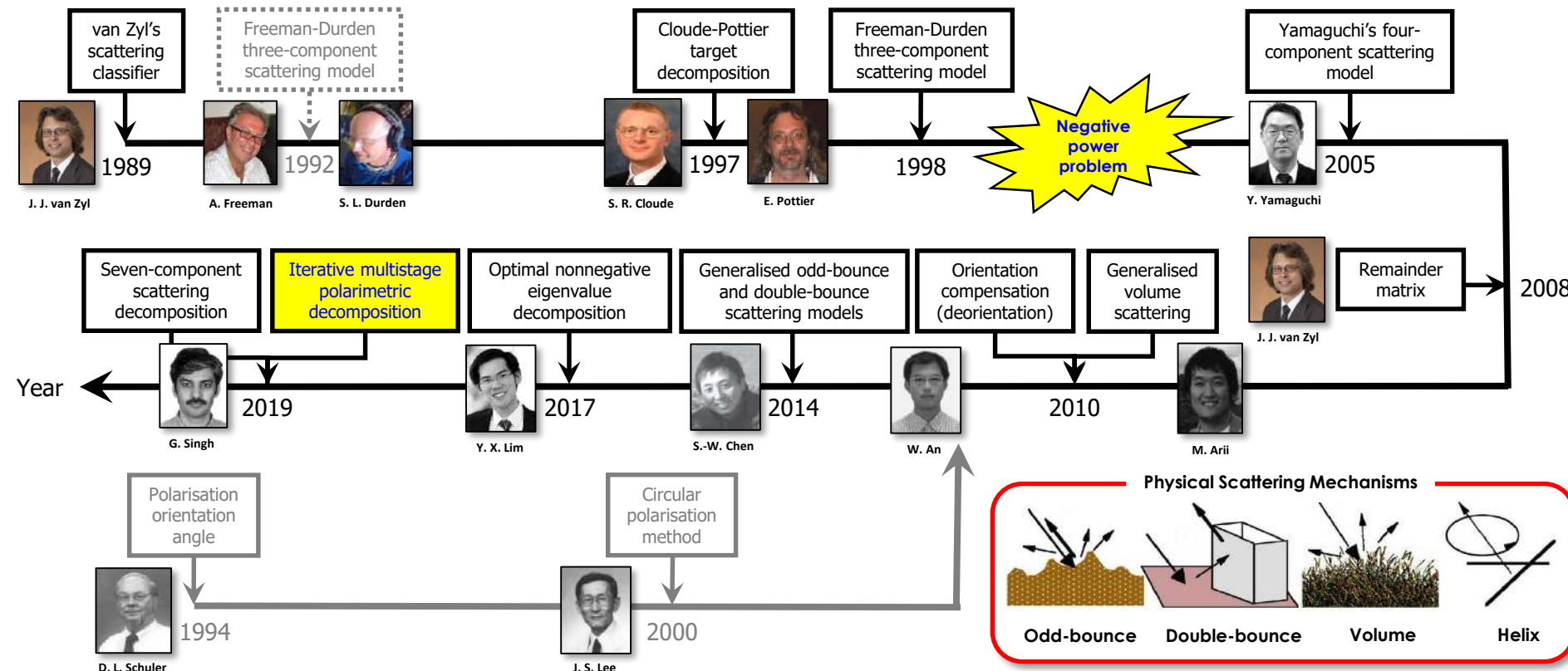
diagonal elements only
 $\sigma = 0.0566$



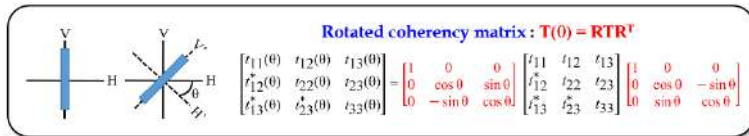
Physical Scattering Decomposition

Physical Scattering Retrieval

- Fully PolSAR data offer valuable opportunities in understanding and quantifying **physical interaction behaviours** between radar waves and the illuminated Earth's surface

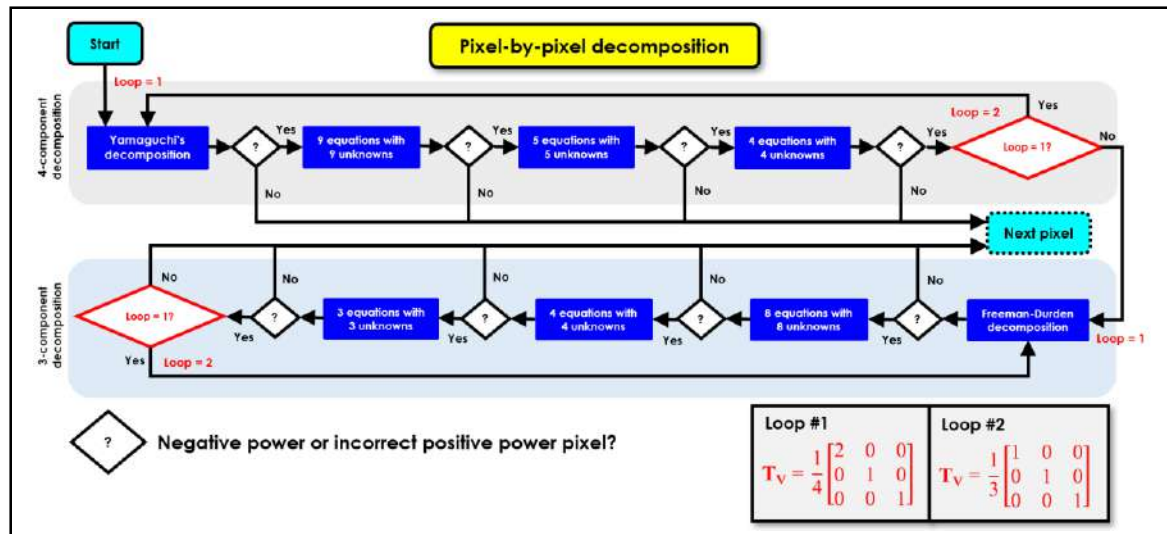
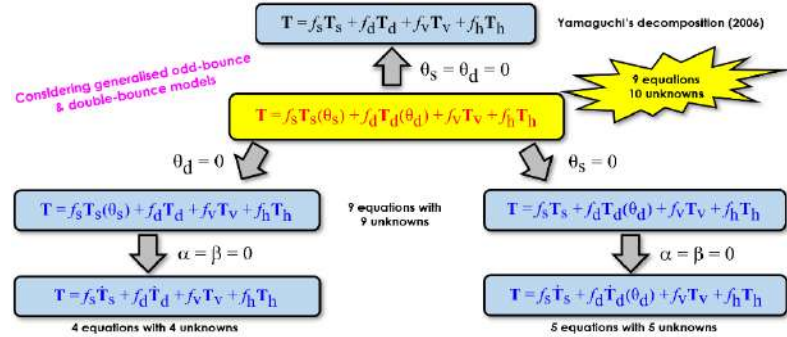


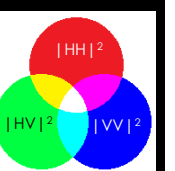
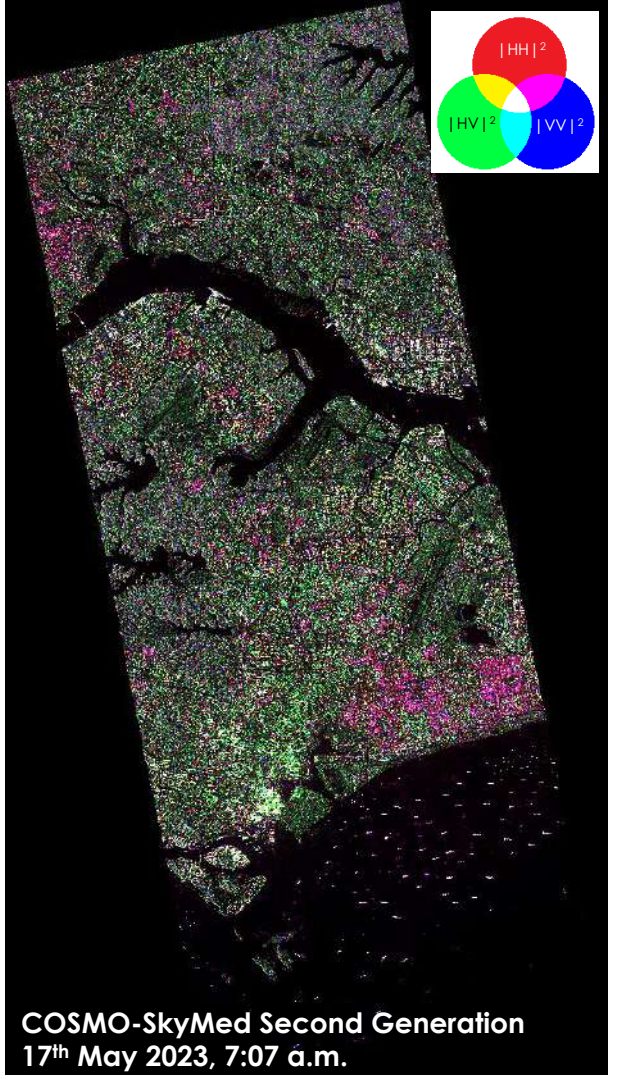
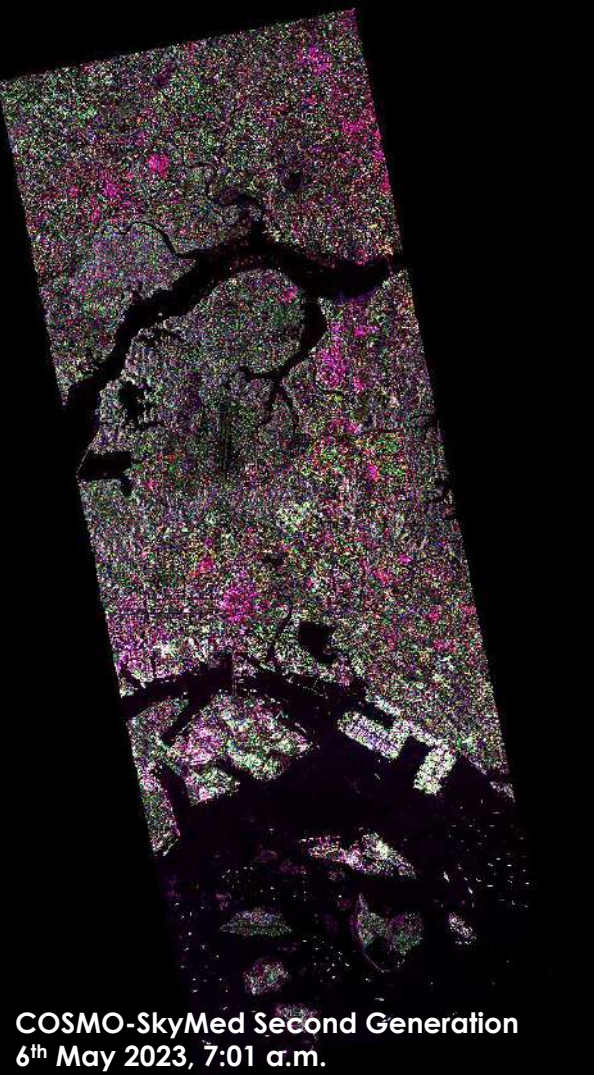
Iterative Multistage Polarimetric Decomposition

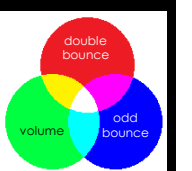
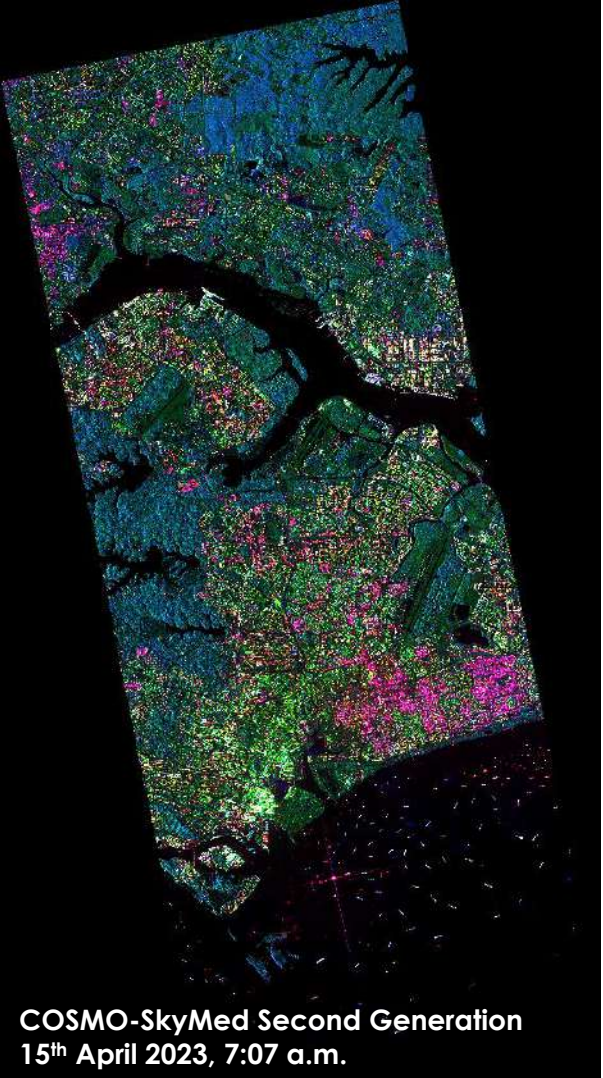


Generalised odd-bounce model $\mathbf{T}_S(\theta_S) - \mathbf{R}\mathbf{T}_S\mathbf{R}^T = f_S \begin{bmatrix} 1 & \beta^* \cos 2\theta_S & -\beta^* \sin 2\theta_S \\ \beta \cos 2\theta_S & |\beta|^2 \cos^2 2\theta_S & -|\beta|^2 \cos 2\theta_S \sin 2\theta_S \\ -\beta \sin 2\theta_S & -|\beta|^2 \cos 2\theta_S \sin 2\theta_S & |\beta|^2 \sin^2 2\theta_S \end{bmatrix}$

Generalised double-bounce model $\mathbf{T}_d(\theta_d) - \mathbf{R}\mathbf{T}_d\mathbf{R}^T = f_d \begin{bmatrix} |\alpha|^2 & \alpha \cos 2\theta_d & -\alpha \sin 2\theta_d \\ \alpha^* \cos 2\theta_d & \cos^2 2\theta_d & -\cos 2\theta_d \sin 2\theta_d \\ -\alpha^* \sin 2\theta_d & -\cos 2\theta_d \sin 2\theta_d & \sin^2 2\theta_d \end{bmatrix}$



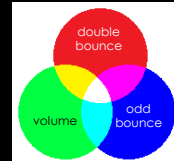
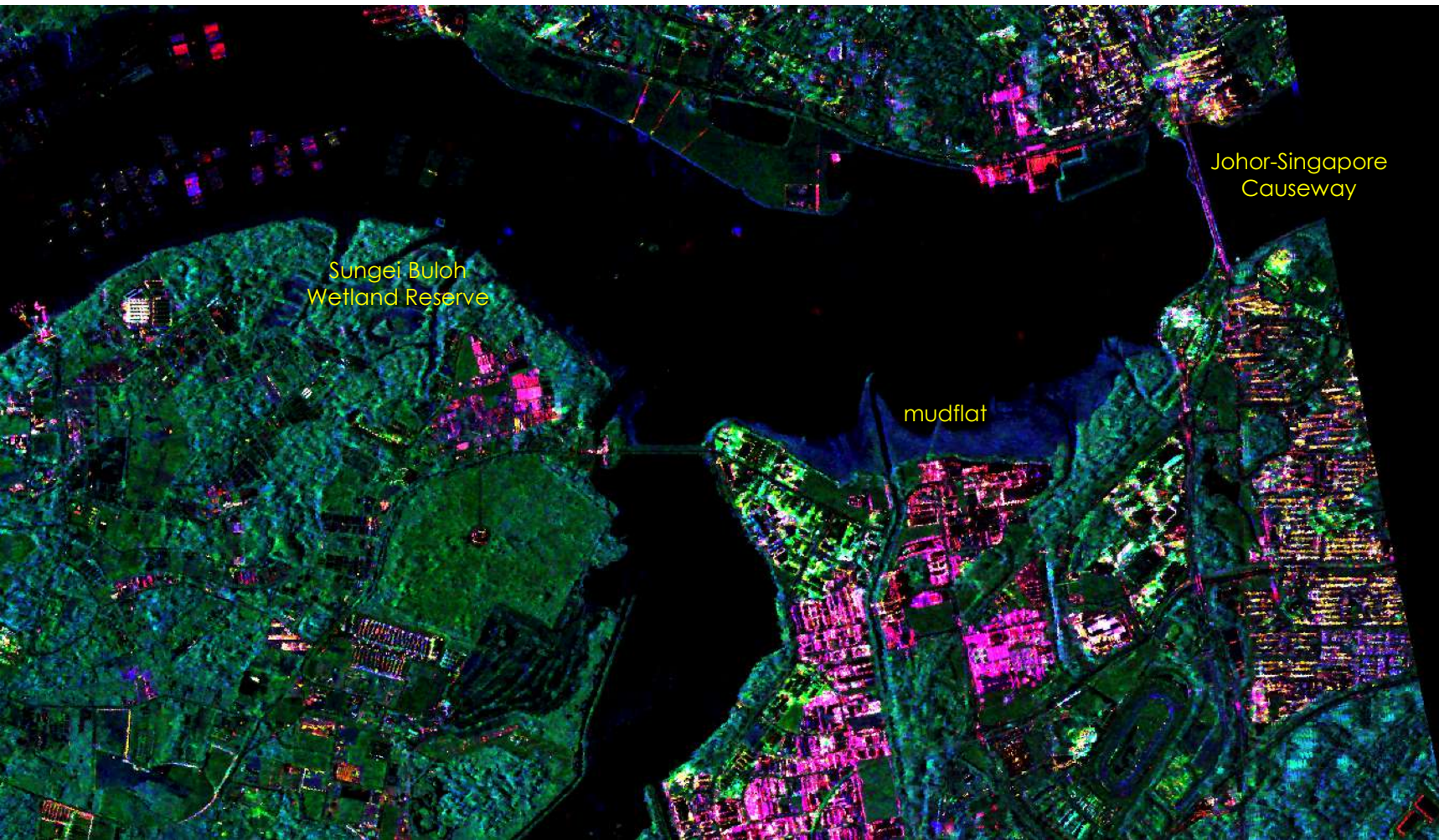




PlanetScope (5th June 2023)



COSMO-SkyMed Second Generation (6th May 2023)



PlanetScope (5th June 2023)



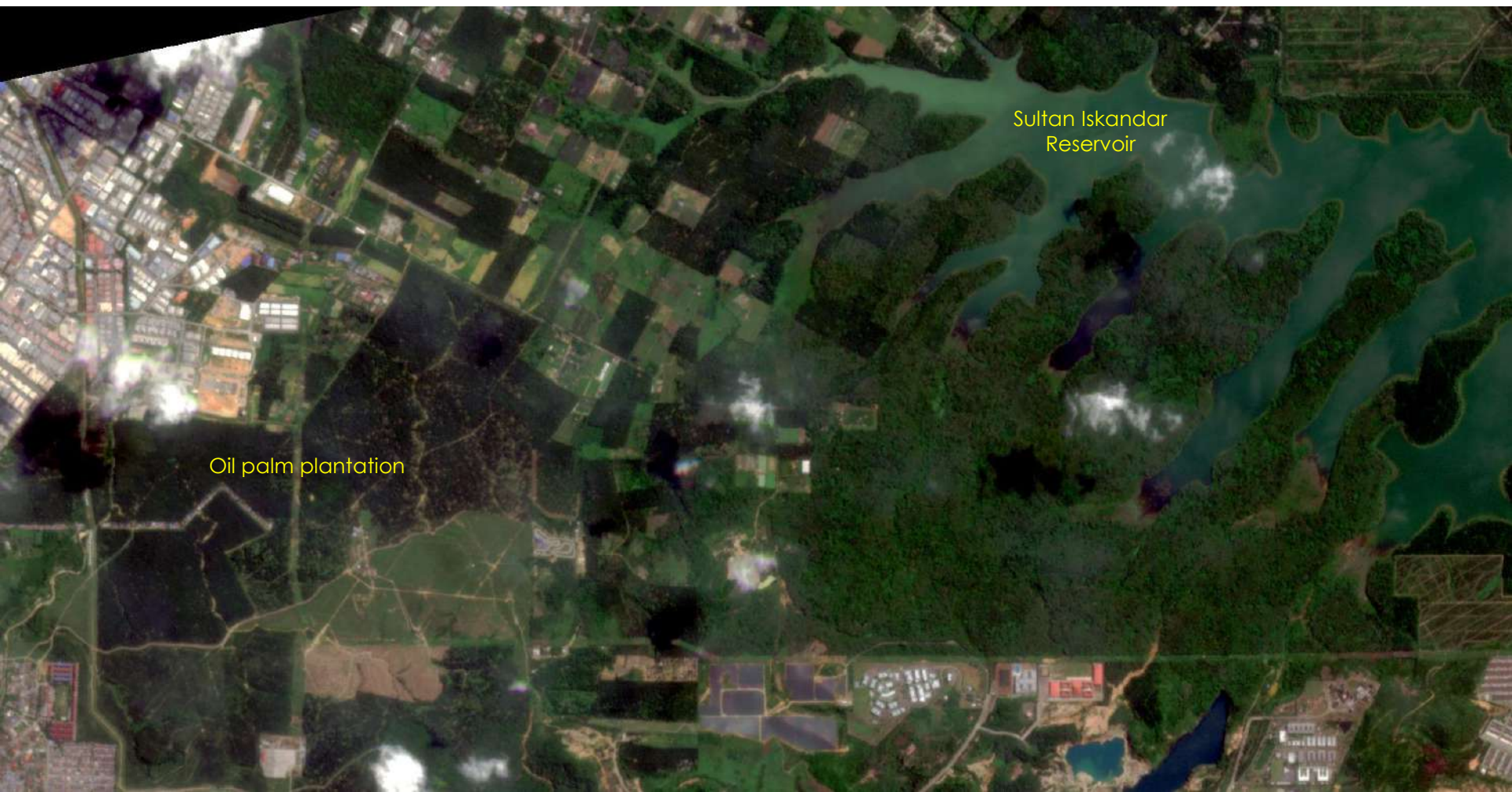
Upper Seletar
Reservoir

Seletar
Airport

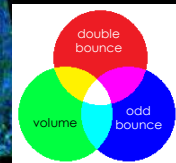
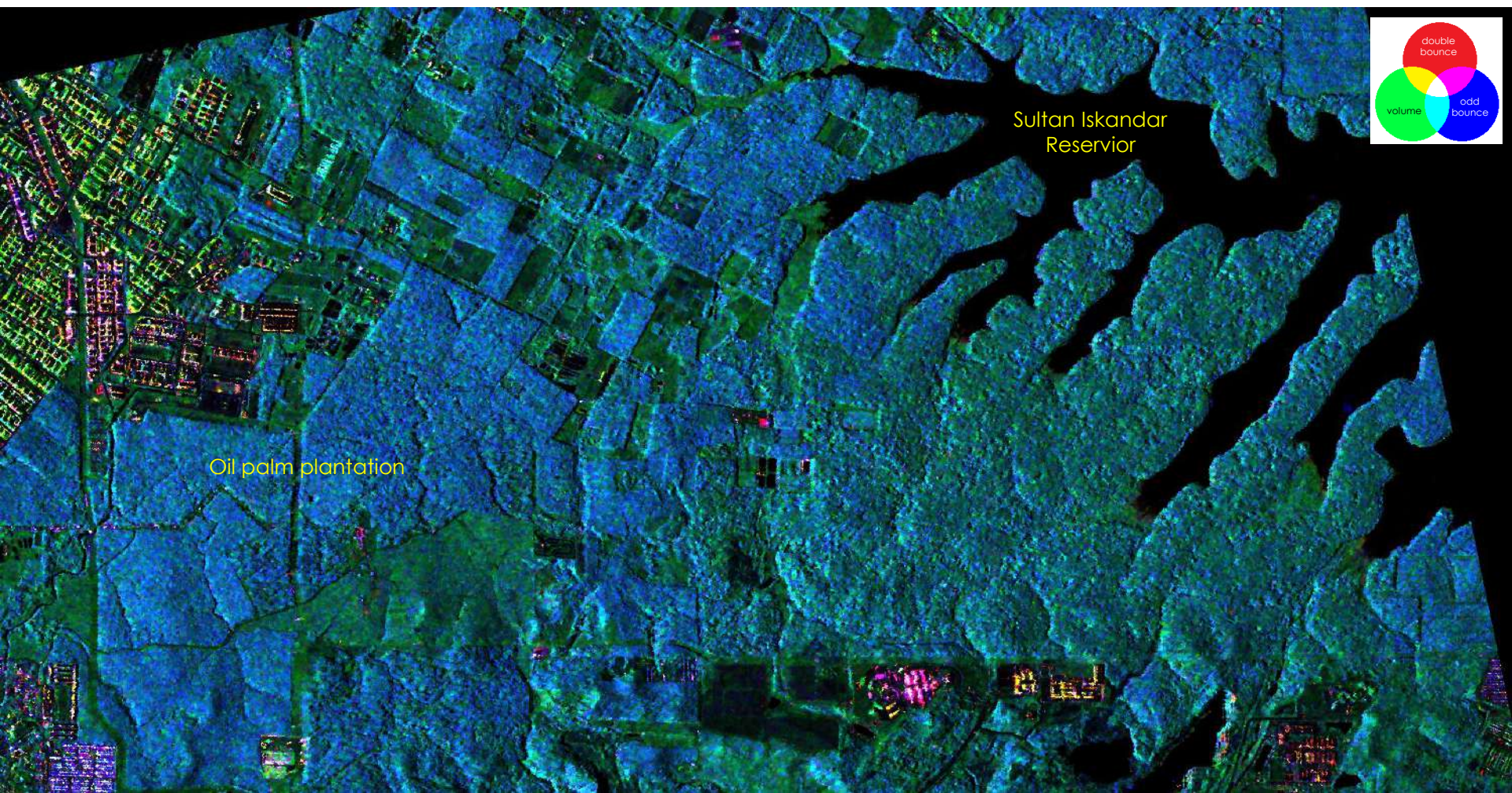
COSMO-SkyMed Second Generation (17th May 2023)



PlanetScope (5th June 2023)

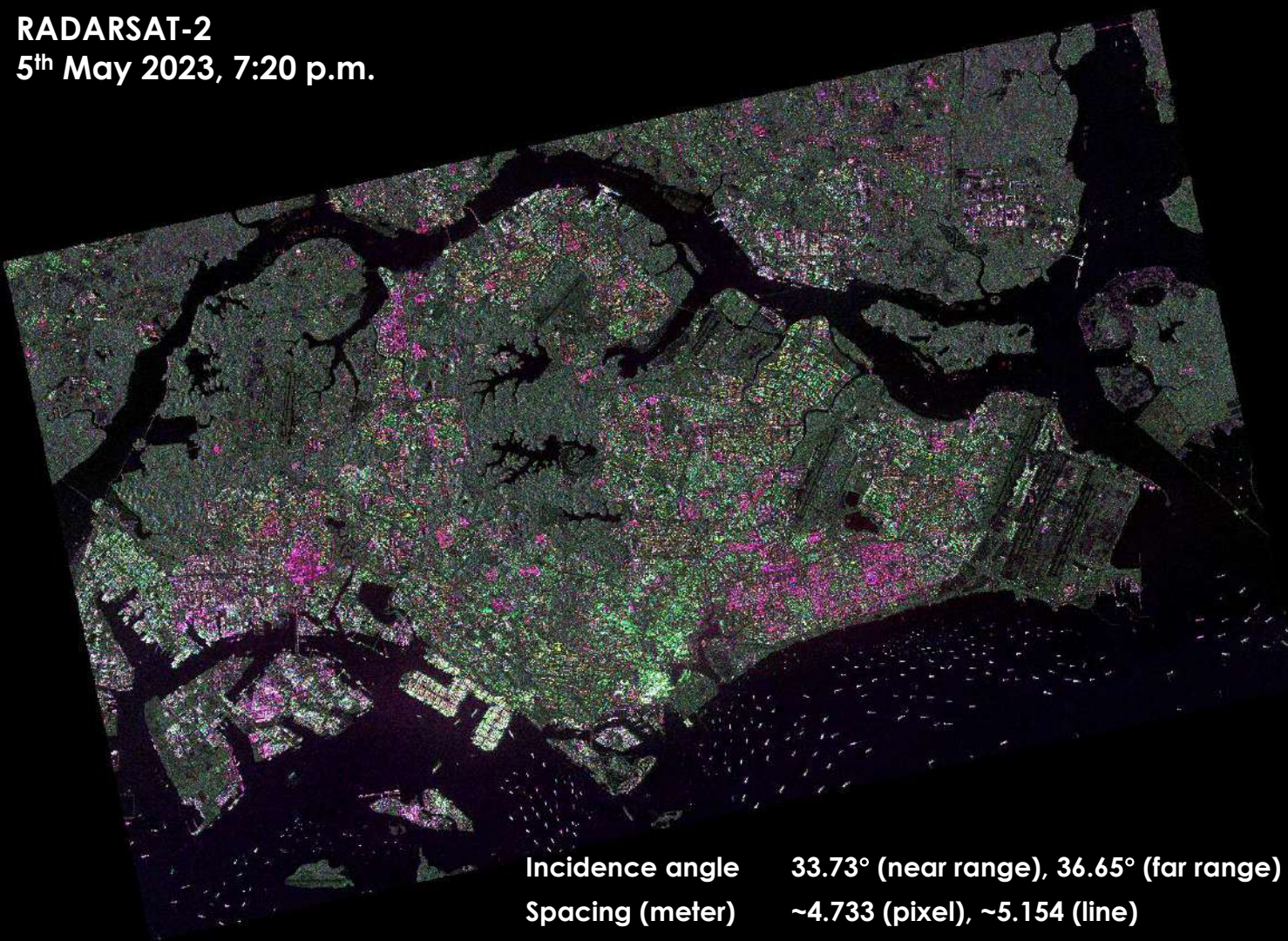


COSMO-SkyMed Second Generation (17th May 2023)

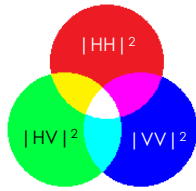


RADARSAT-2

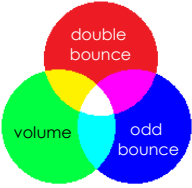
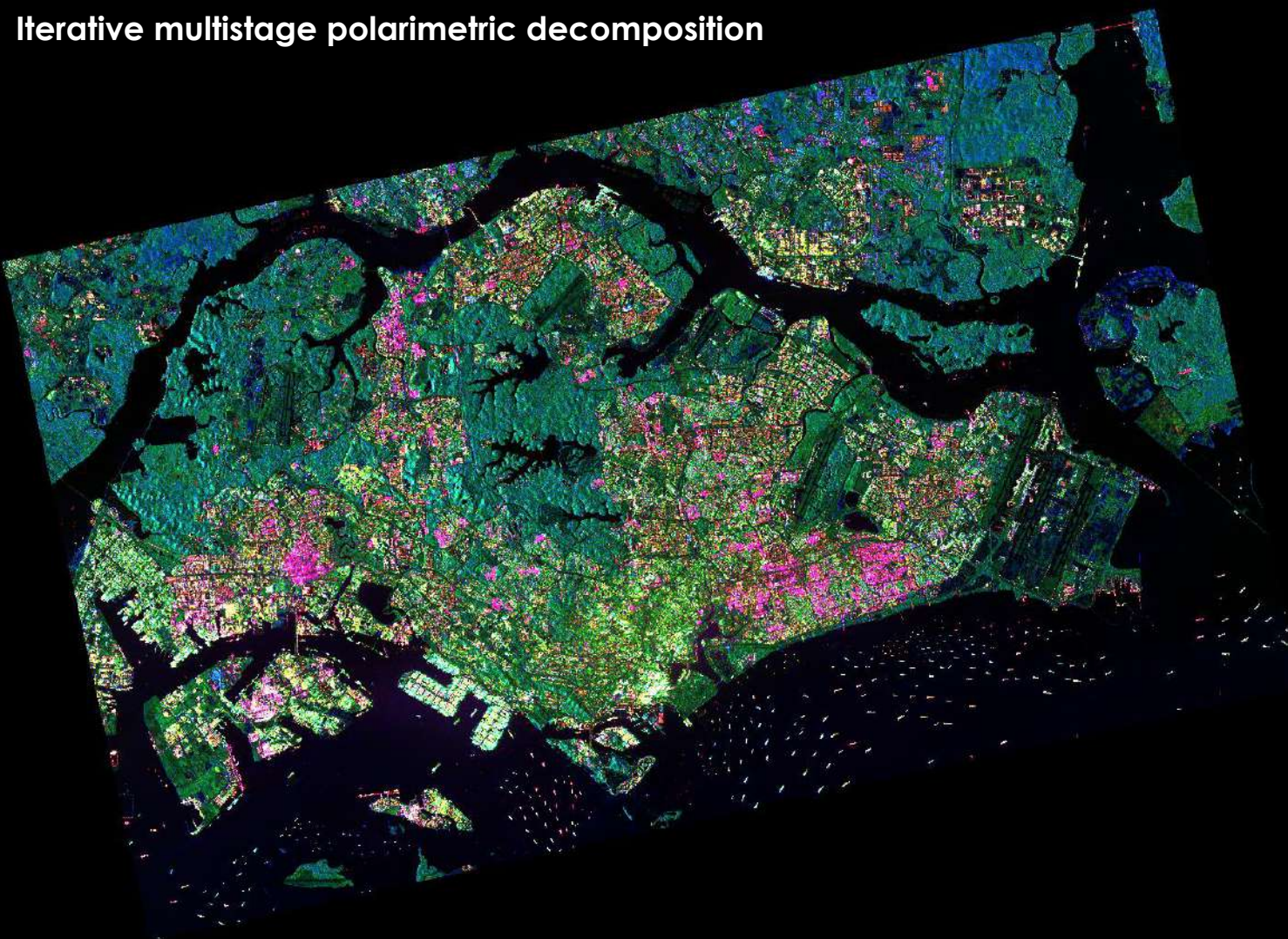
5th May 2023, 7:20 p.m.



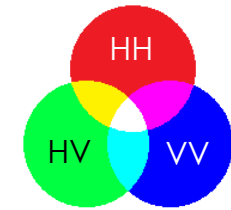
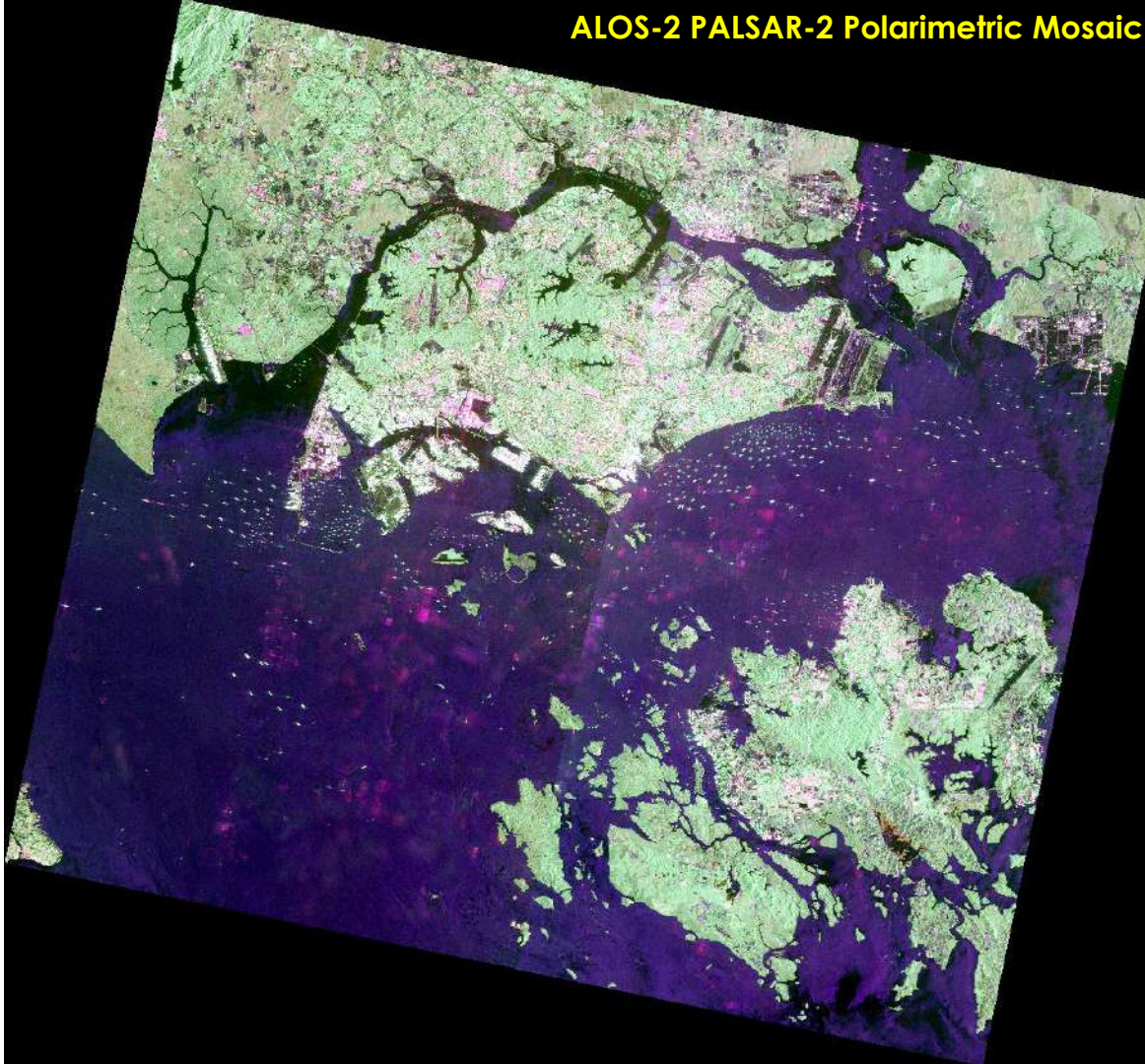
Incidence angle 33.73° (near range), 36.65° (far range)
Spacing (meter) ~4.733 (pixel), ~5.154 (line)

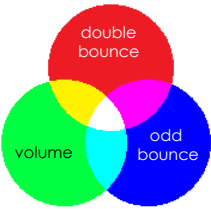


Iterative multistage polarimetric decomposition



ALOS-2 PALSAR-2 Polarimetric Mosaic





Odd-bounce

- bare land, sea surface

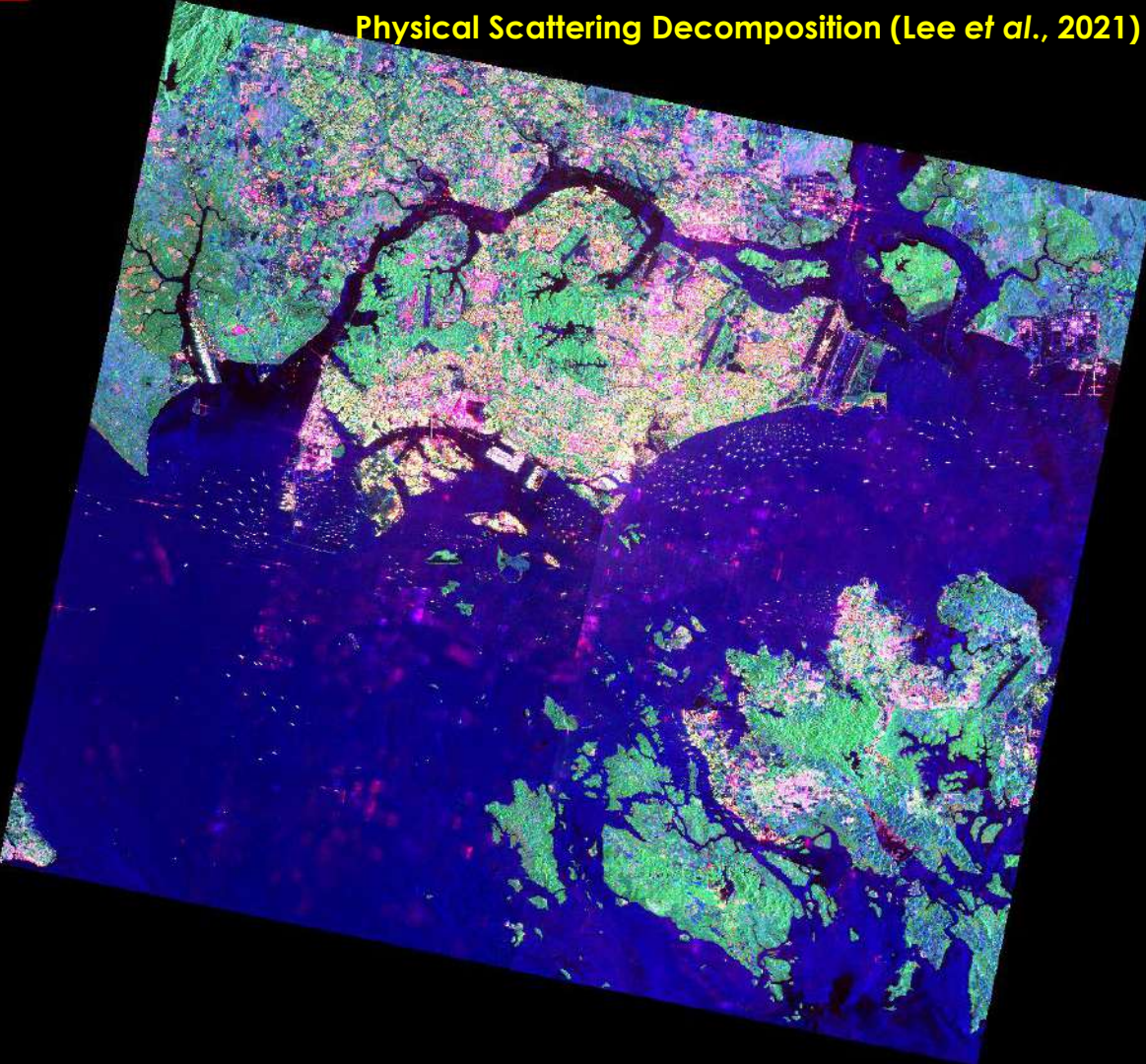
Double-bounce

- built-up area

Volume scattering

- forest

Physical Scattering Decomposition (Lee et al., 2021)



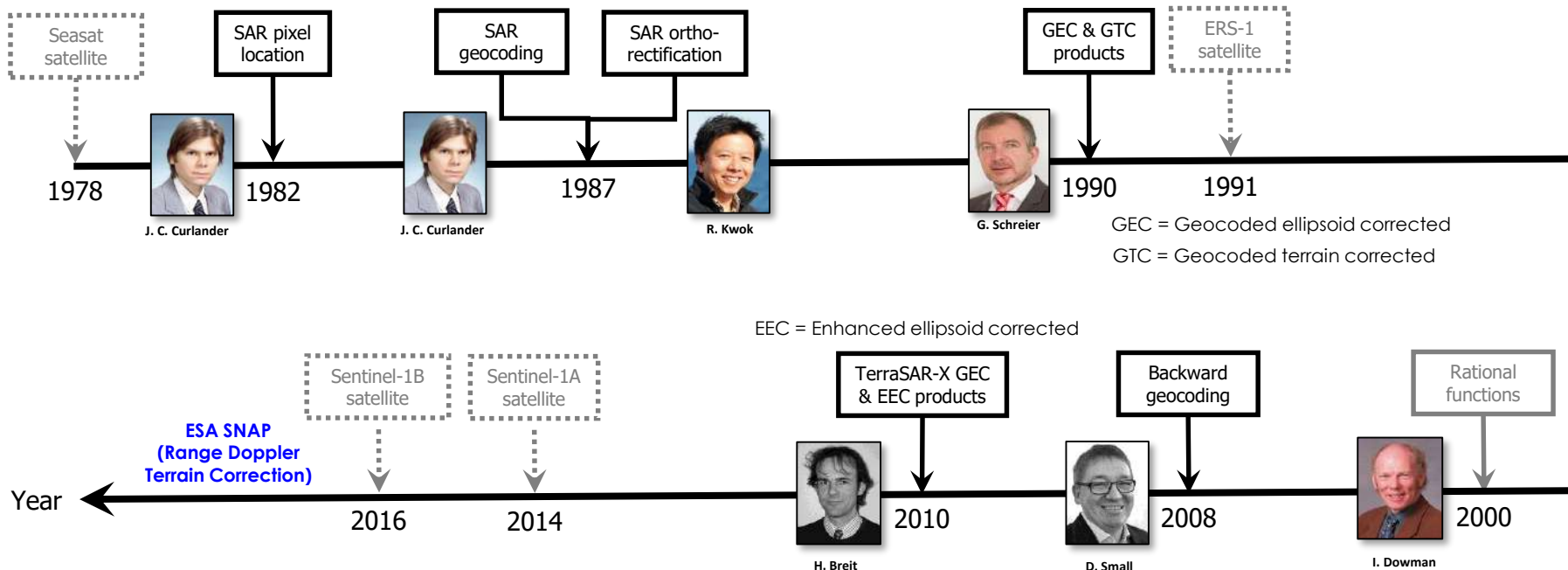
Total number of negative power pixels reduced to ~ 0.006% (9114 pixels)

K. Y. Lee, C. G. Hou, S. C. Liew, and L. K. Kwok (2021). Speckle filtering and physical scattering decomposition for ALOS-2 PALSAR-2 polarimetric mosaic. Proc. ACRS, paper no. ACRS21_029.

Orthorectification

Geocoding and Orthorectification for SAR Images

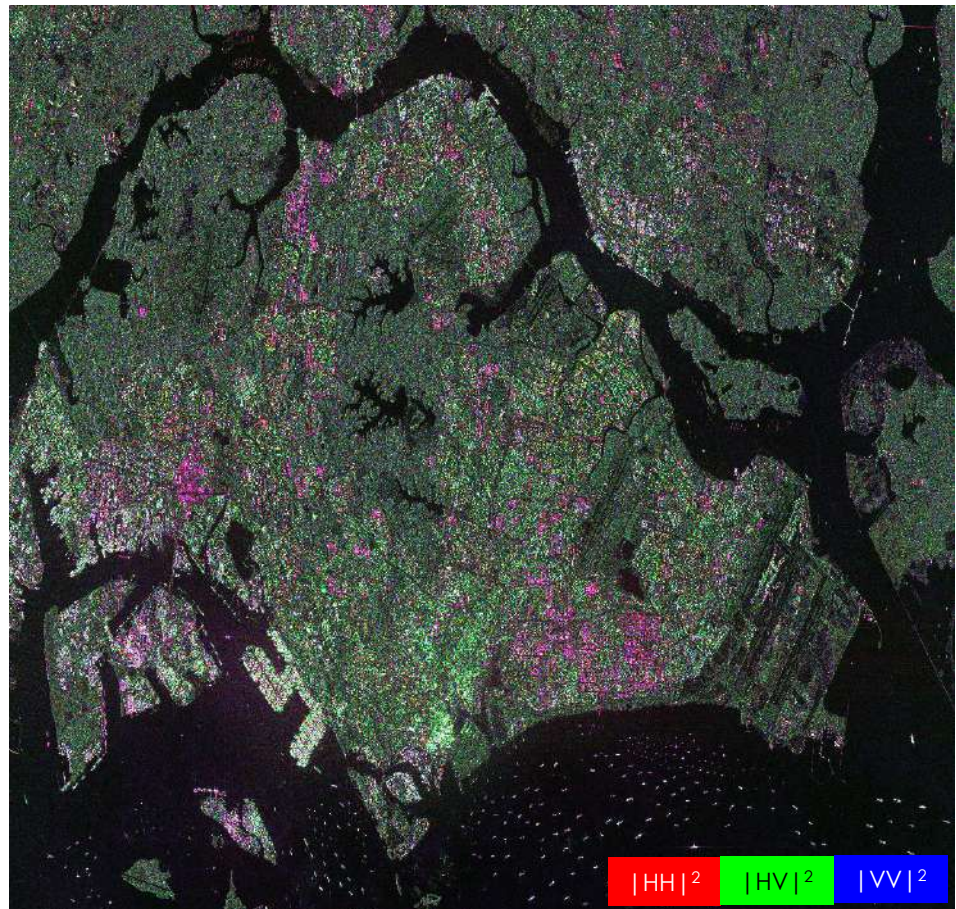
- Geocoding = process of resampling image data for conforming to a map grid
- Orthorectification = geometric rectification of image data with terrain correction



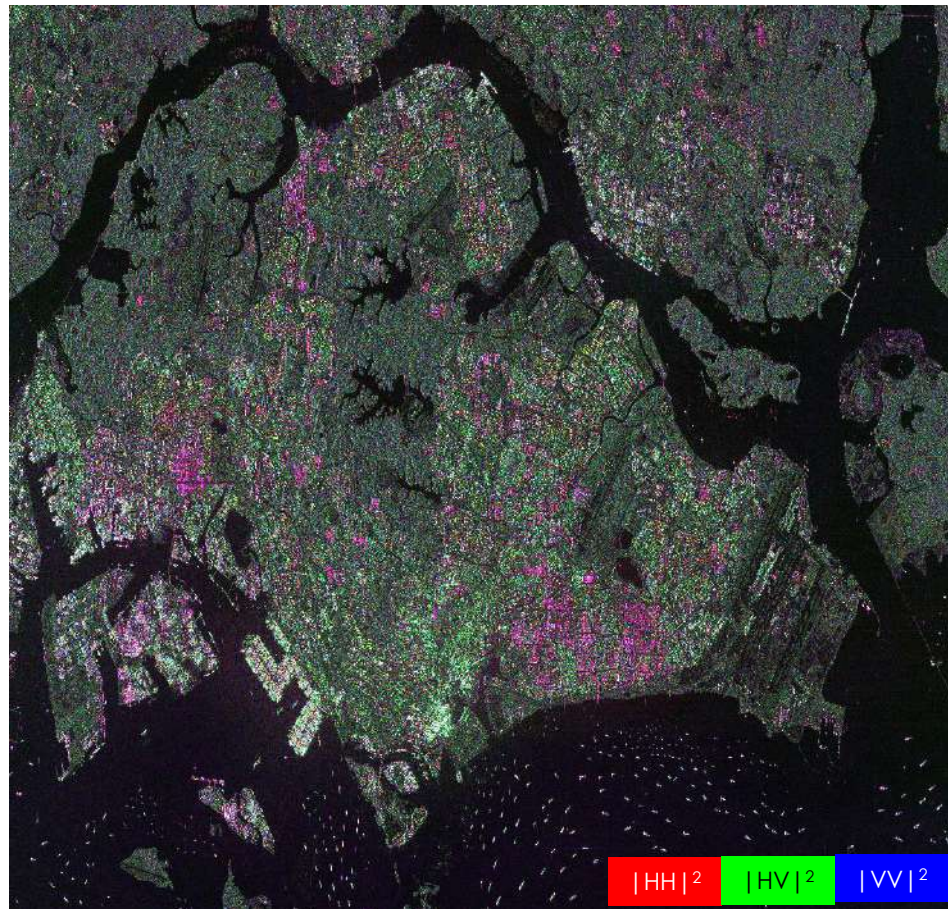
J. C. Curlander and R. N. McDonough (1991). *Synthetic Aperture Radar: Systems and Signal Processing*. New York: John Wiley.

F. W. Leberl (1990). *Radargrammetric Image Processing*. Norwood: Artech House.

RADARSAT-2 SLC Data Over Singapore



1st October 2022 UTC



5th May 2023 UTC

Orthorectified RADARSAT-2 (1st October 2022 UTC)

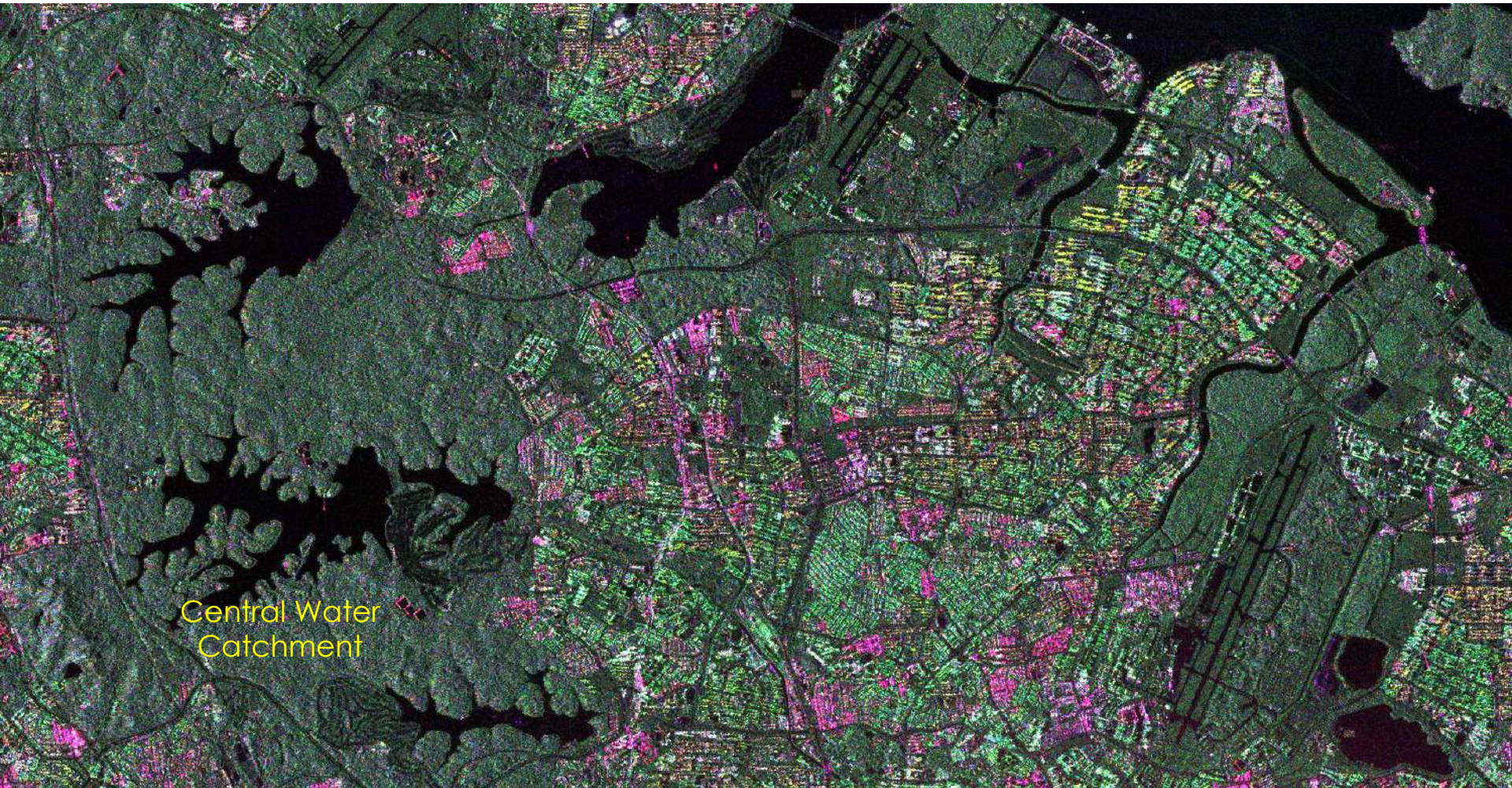


Orthorectified RADARSAT-2 (5th May 2023 UTC)

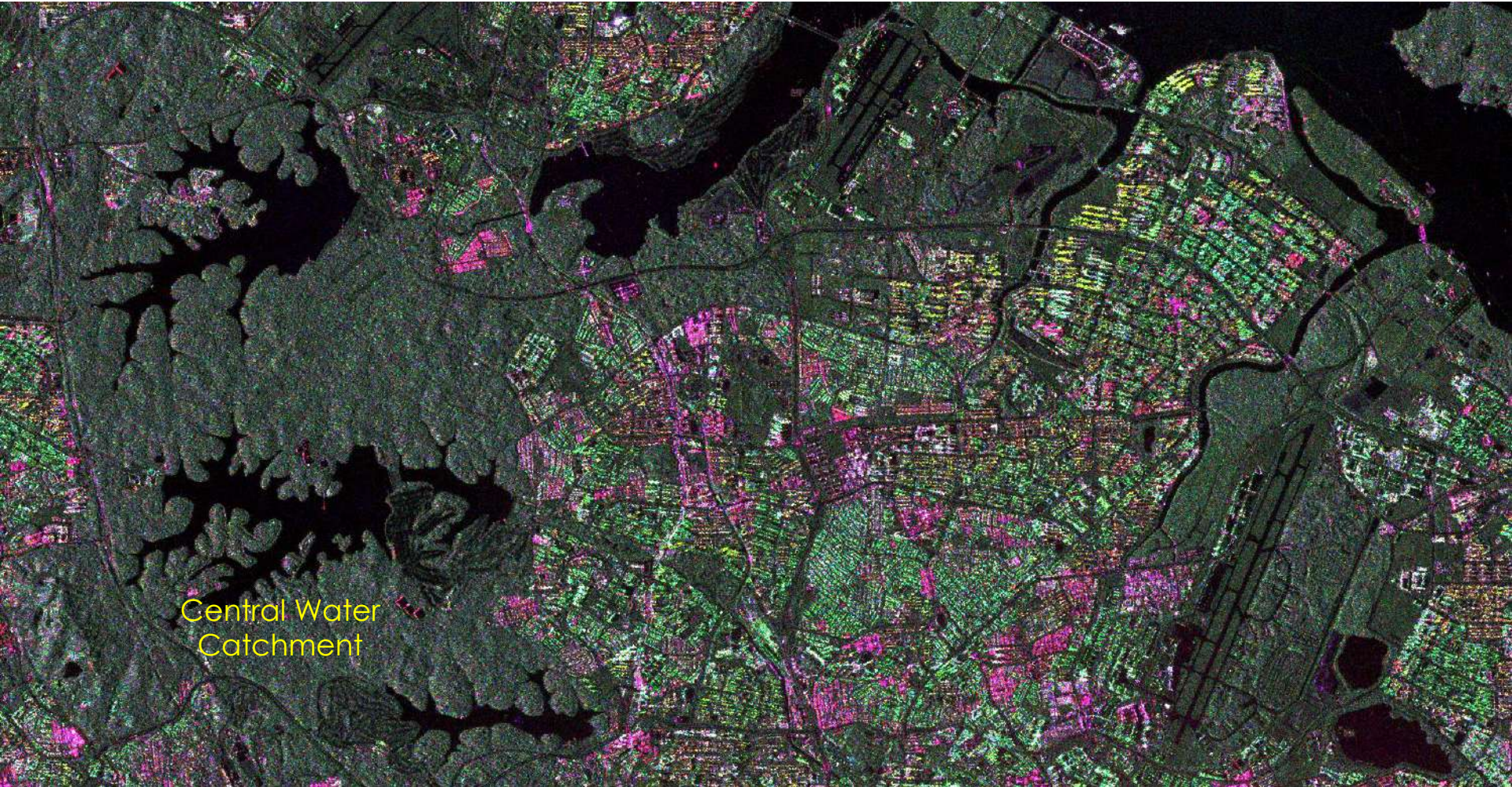


Sentinel-2 (30th January 2022)





RADARSAT-2 (5th May 2023 UTC)



Sentinel-2 (25th January 2022)



RADARSAT-2 (1st October 2022 UTC)



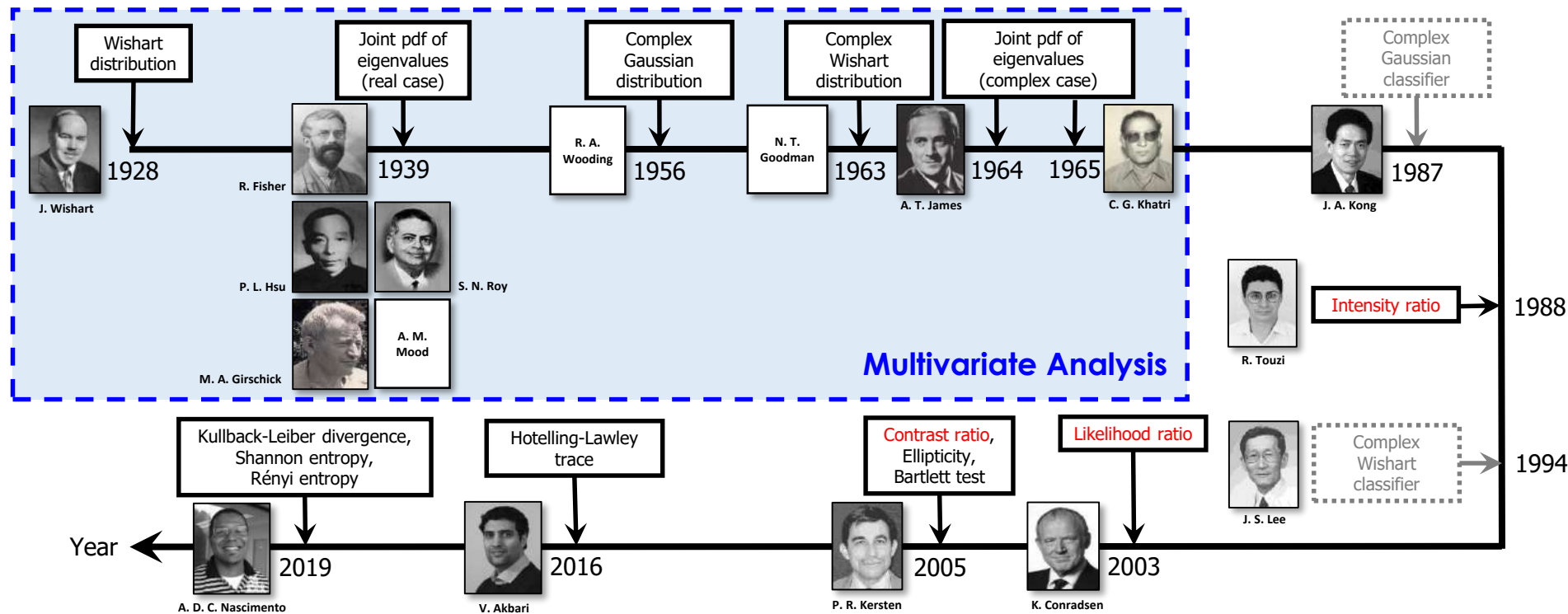
RADARSAT-2 (5th May 2023 UTC)



Change Detection

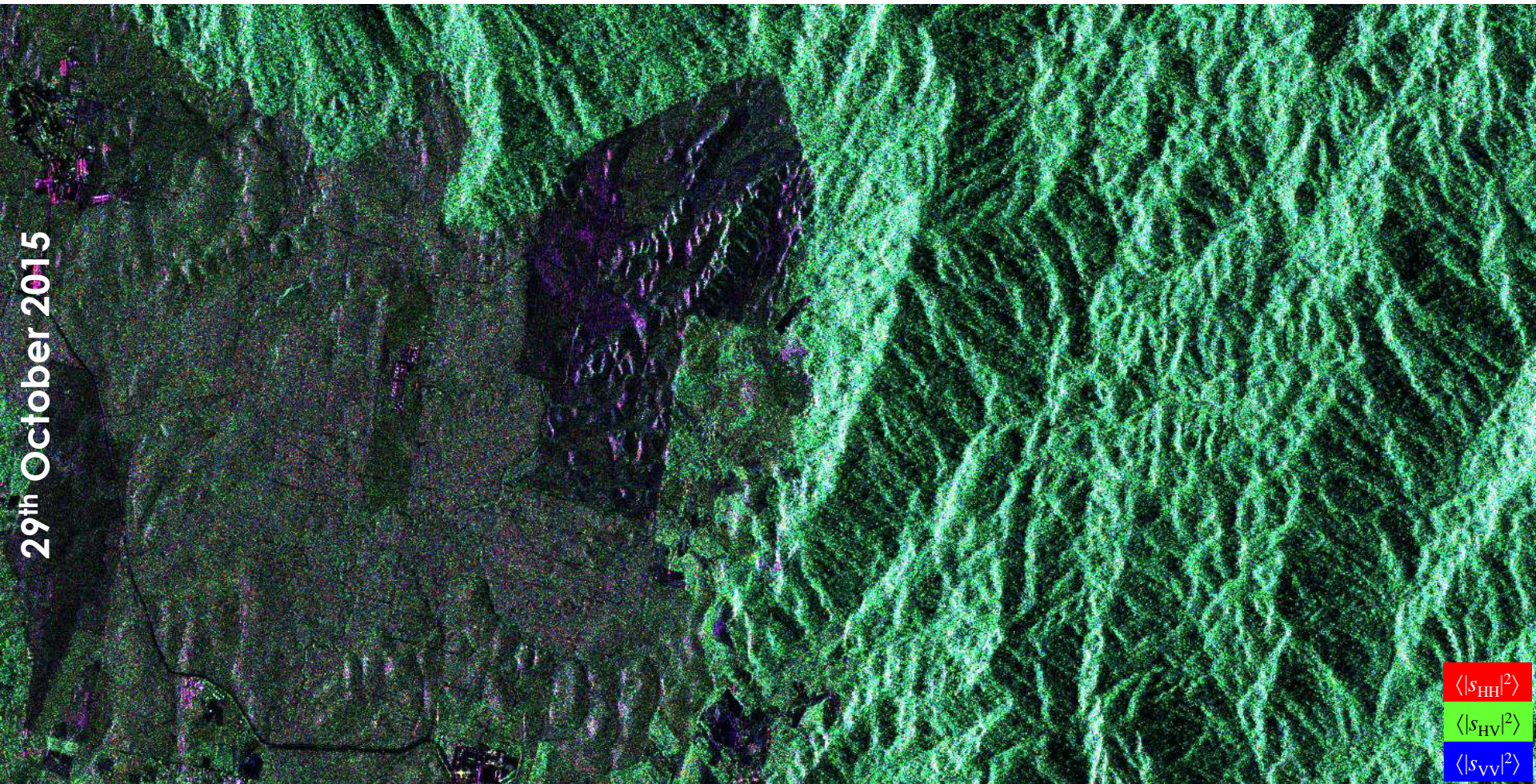
Change Detection

- Change detection using multi-temporal remotely sensed data is a very important application for environmental monitoring, disaster management etc.
- Statistical approaches have prevailed in polarimetric change detection



ALOS-2 PALSAR-2 Over Kampung Ulu Mahang

29th October 2015



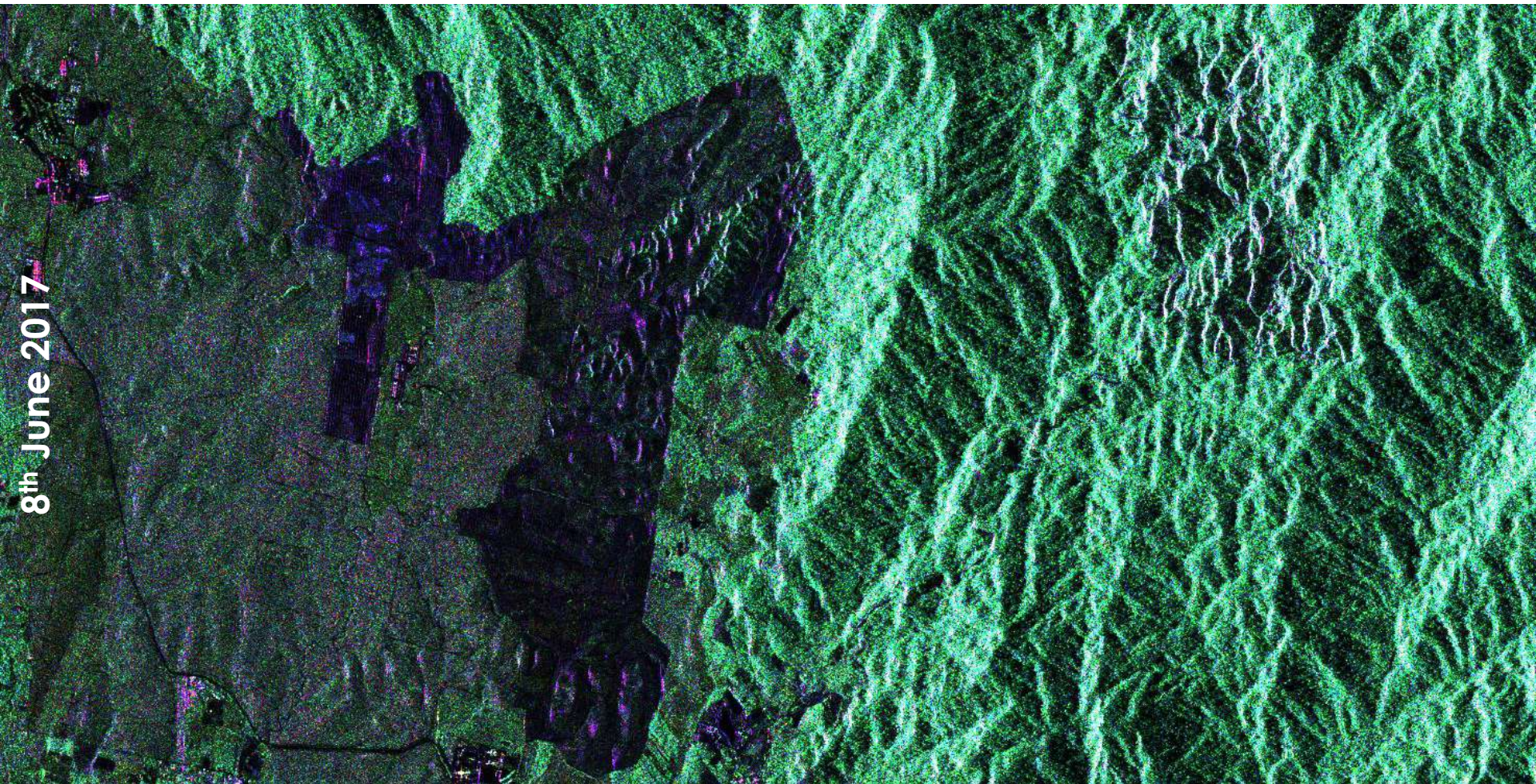
$\langle |s_{\text{HH}}|^2 \rangle$

$\langle |s_{\text{HV}}|^2 \rangle$

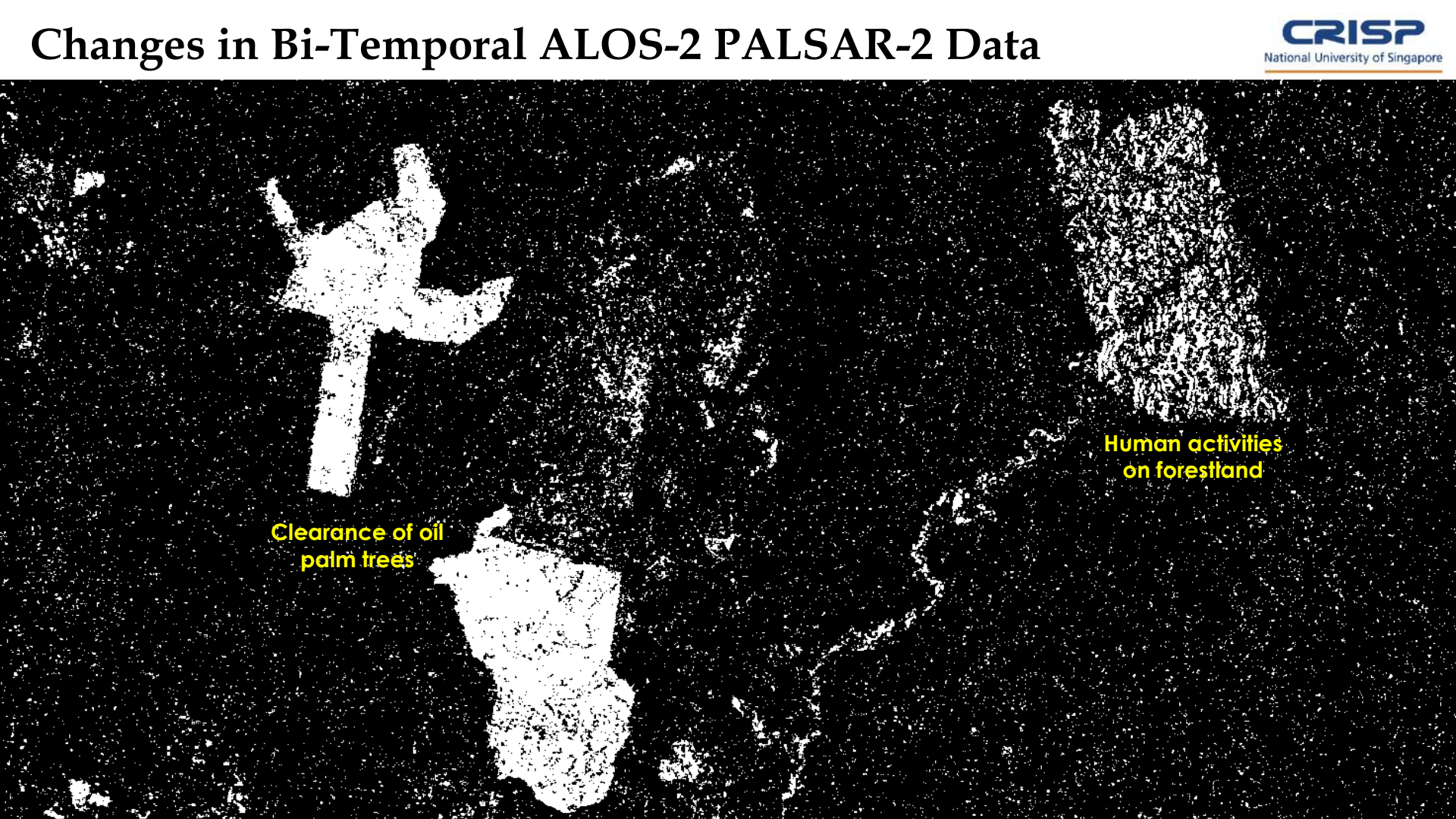
$\langle |s_{\text{VV}}|^2 \rangle$

ALOS-2 PALSAR-2 Over Kampung Ulu Mahang

8th June 2017



Changes in Bi-Temporal ALOS-2 PALSAR-2 Data



A grayscale satellite image showing land cover changes over time. The image is heavily textured and grainy. Two specific areas are highlighted with white outlines and labeled in yellow text. On the left, a large area of cleared land is labeled "Clearance of oil palm trees". On the right, a more irregularly shaped area is labeled "Human activities on forestland". The background consists of dark, heavily shaded terrain.

Clearance of oil
palm trees

Human activities
on forestland

ALOS-2 PALSAR-2 Over Padang Serai Town

29th October 2015

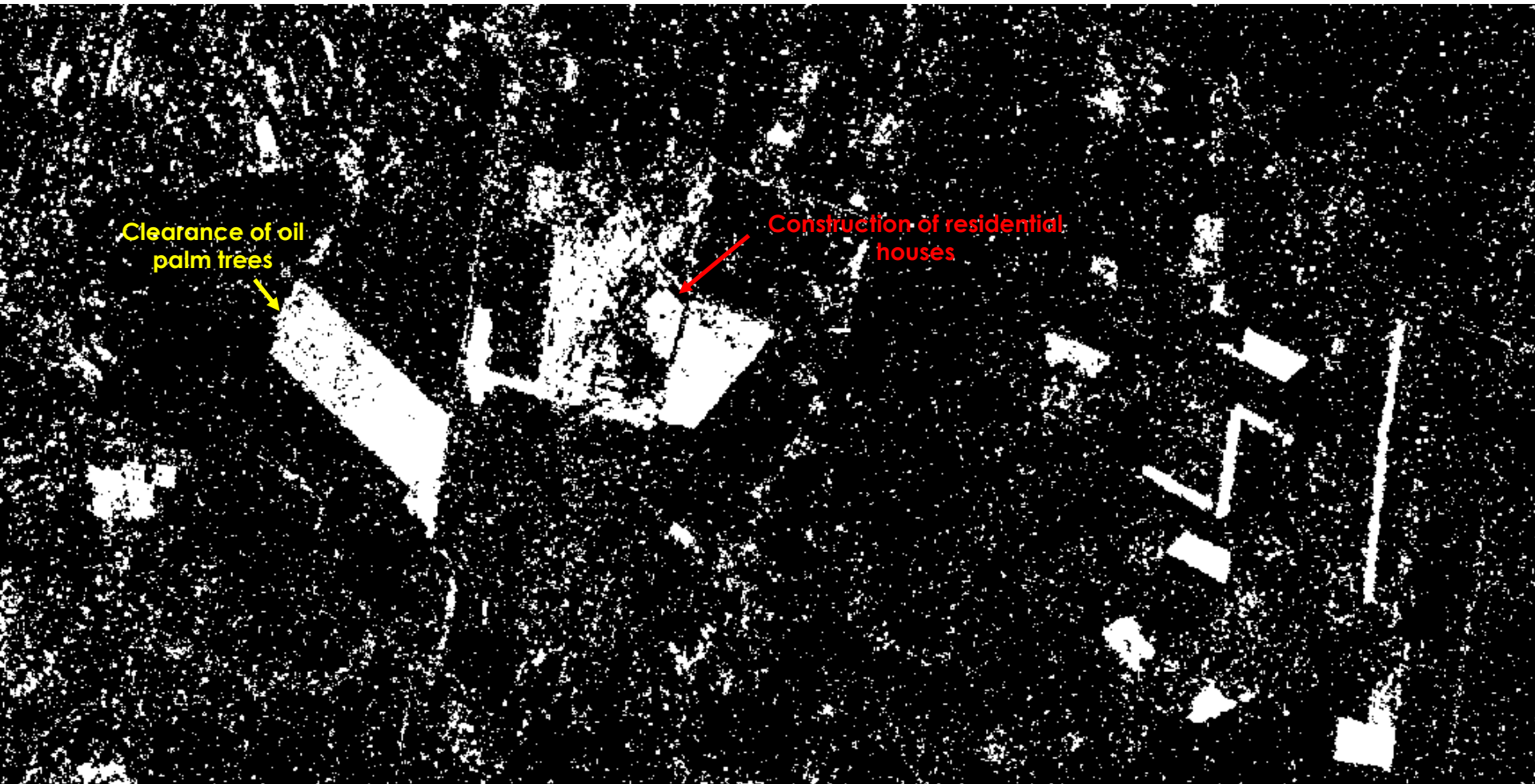


ALOS-2 PALSAR-2 Over Padang Serai Town

8th June 2017

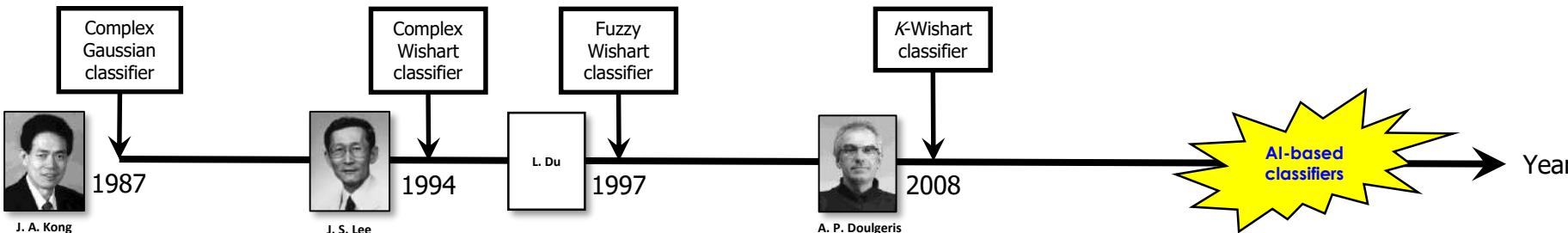


Changes in Bi-Temporal ALOS-2 PALSAR-2 Data

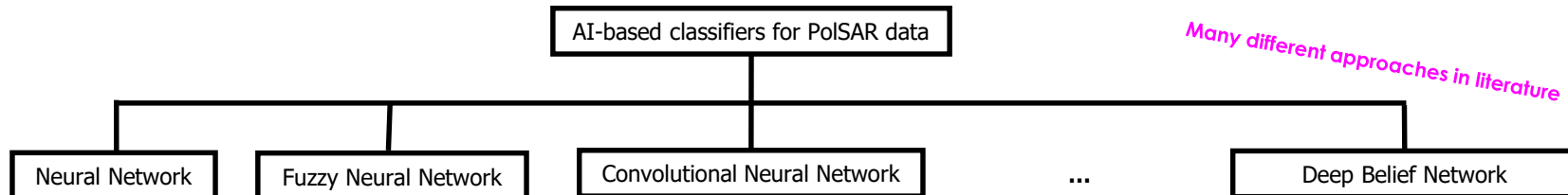


Land Cover Classification

Polarimetric Classification



- **Statistical pattern recognition**, which is based on **statistical distribution**
 - Homogeneous model : Complex Wishart classifier (Lee et al., 1994)
 - Texture model : K-Wishart classifier etc.
- **Artificial intelligence**, where **no assumption** is made on the underlying data distribution

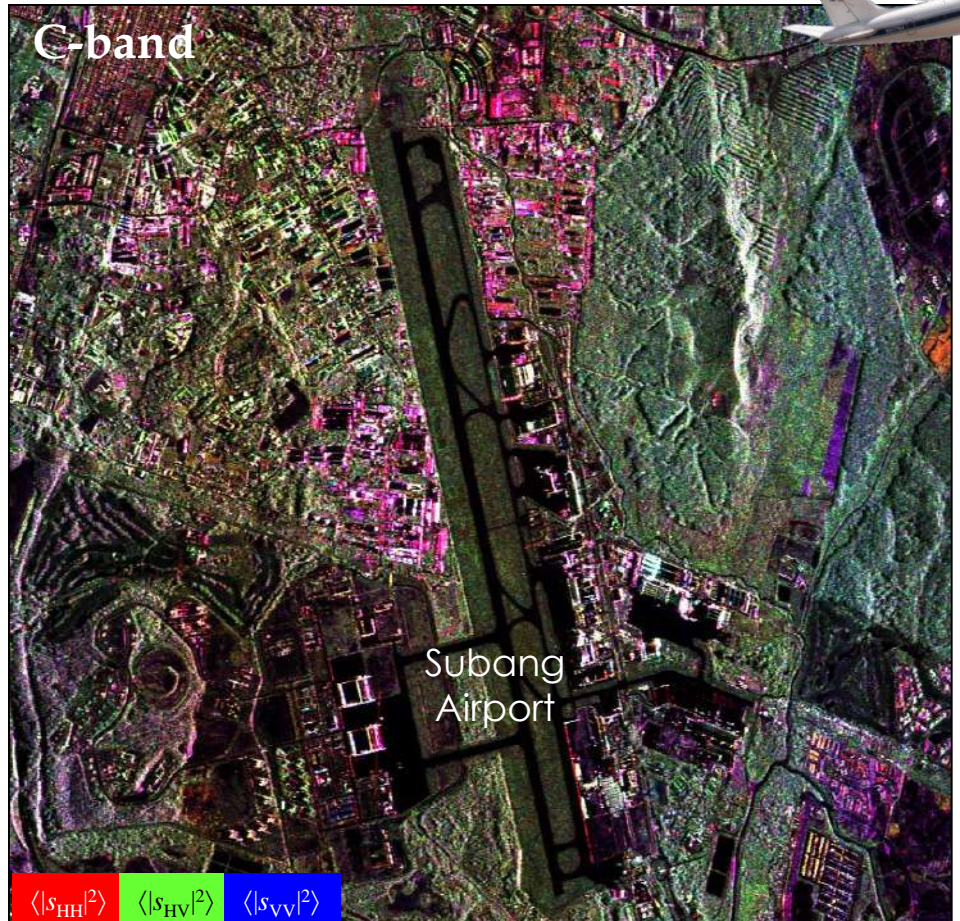


NASA/JPL AIRSAR Data

DC-8 Aircraft

CRISP
National University of Singapore

C-band

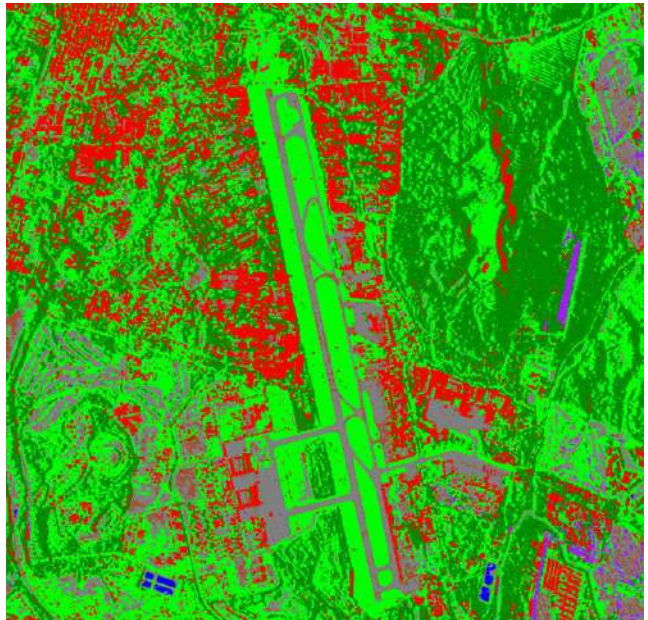


L-band

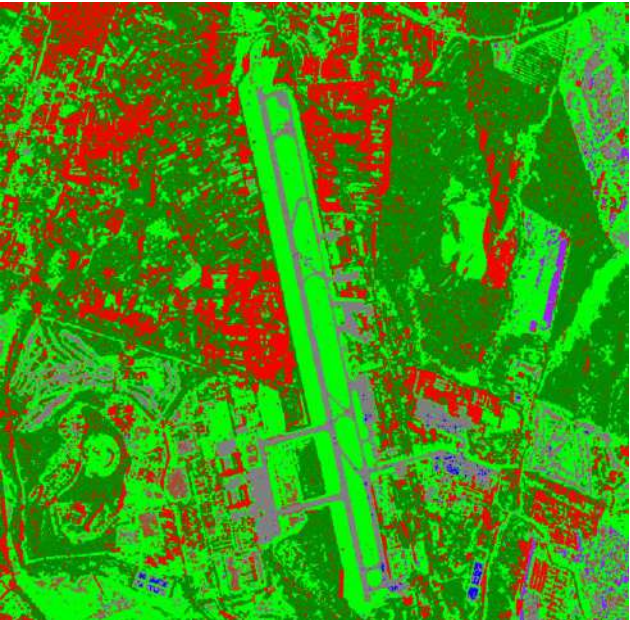


Complex Wishart Classifier

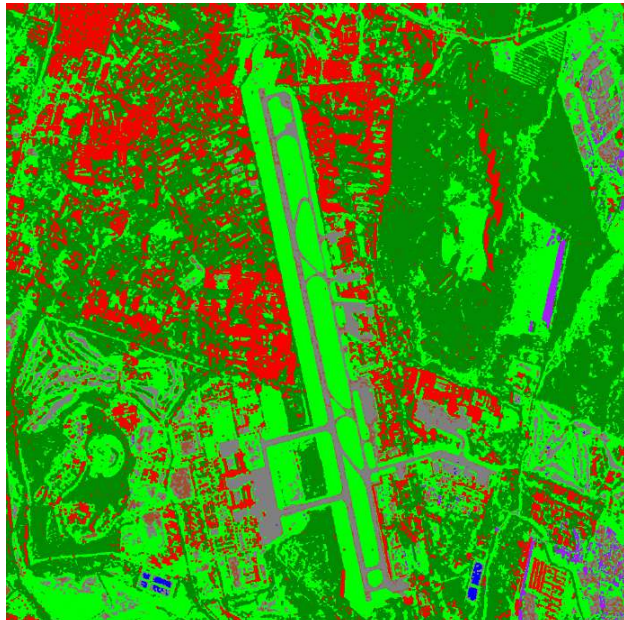
C-band



L-band



C+L bands



Bare land

Grassland / shrub

Man-made

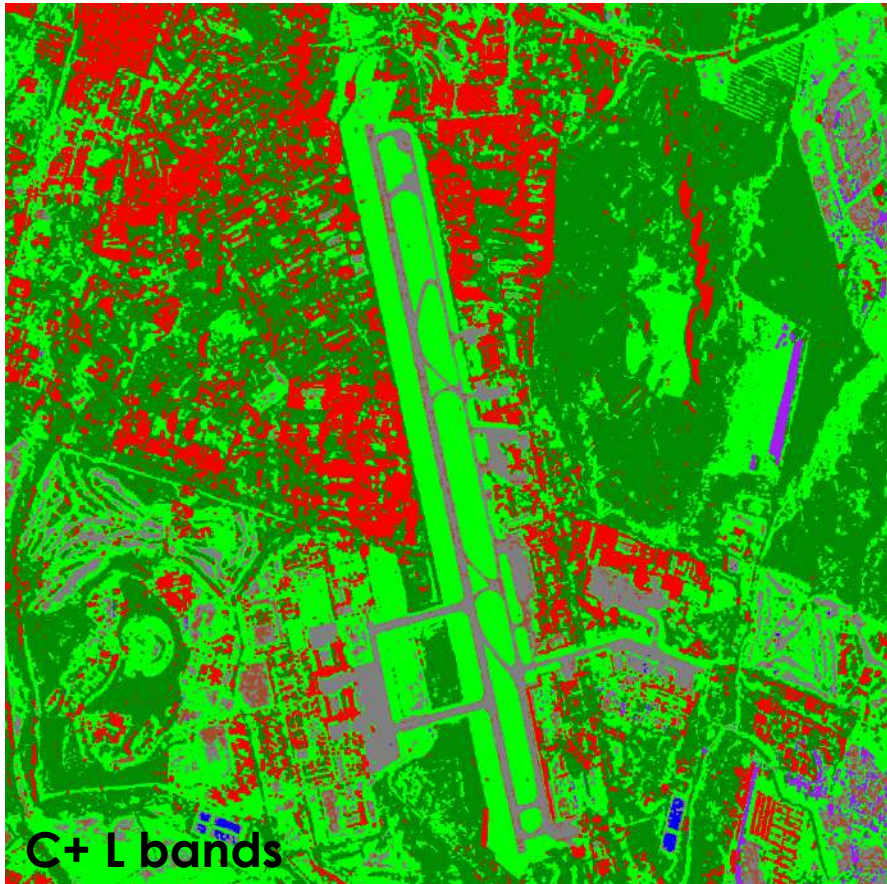
Plantation

Runway

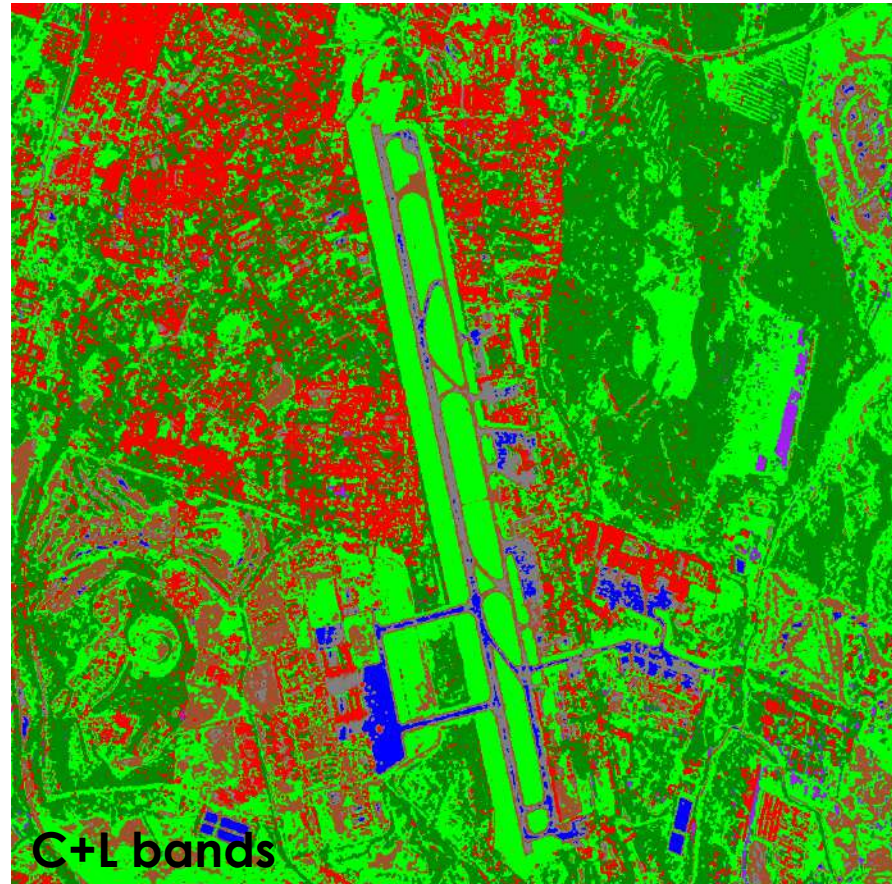
Tree cover

Waterbody

Comparison to Neural Network

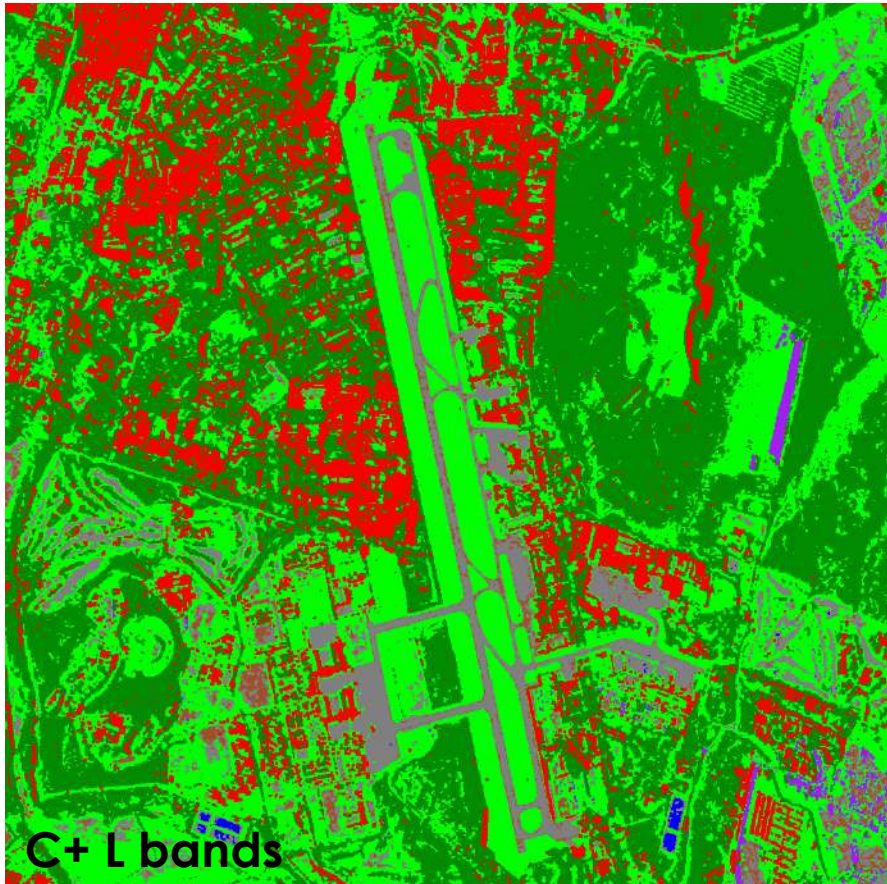


Complex Wishart Classifier



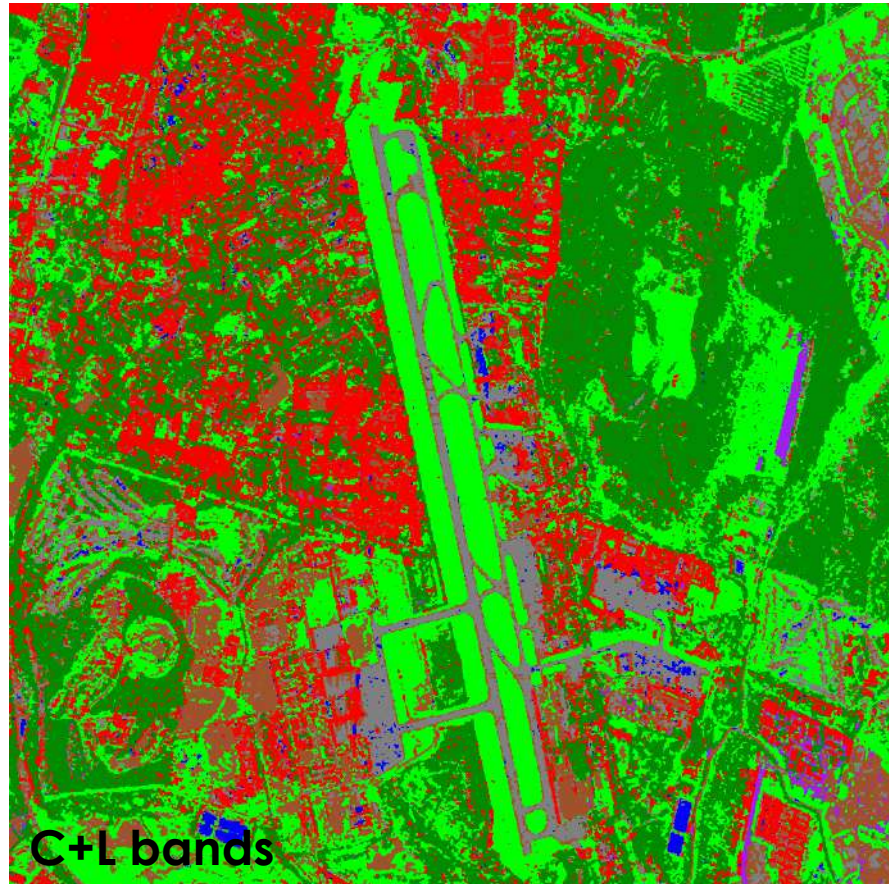
Neural Network

Comparison to Convolutional Neural Network



C+L bands

Complex Wishart Classifier



C+L bands

Convolutional Neural Network

Land Deformation Monitoring

Interferometric SAR Research and Development

□ Project : **Fully Automatic Processing Framework for Persistent Scatterer Interferometry (PS-InSAR)**

□ Lead investigator : Dr. Chen Guang HOU
(email: crshc@nus.edu.sg)

□ NUS IT HPC (<https://nusit.nus.edu.sg/hpc/>):

- Up to 96 CPU cores
- Up to 375 GB RAM
- 500 GB space

□ Project deliverables :

- Fully automated PS-InSAR processing system
- Academic publication (1 conference paper)
- Local capacity building on PS-InSAR processing of Sentinel-1 time series (i.e., 2 CRISP staff)
- Knowledge sharing with 

FULLY AUTOMATIC PERSISTENT SCATTERER INTERFEROMETRY PROCESSING FRAMEWORK USING SNAP, STAMPS AND HIGH PERFORMANCE COMPUTING

Chen Guang HOU, Kew Hong LEE, Sow Chin LIEW and Leong Keong KWOK

Centre for Remote Imaging, Sensing and Processing
National University of Singapore

ABSTRACT

An efficient tool to investigate time series of ground deformation resulting from human activities or natural disasters, persistent scatterer (PS) interferometry requires a large amount of computing resources especially for the processing time series of multi-sensor and multi-temporal images. In this paper, we propose a fully automatic PS-InSAR processing framework using the open source software packages including the Sentinel Application Platform (SNAP) from ESA and the Standard Method of Persistent Scatterer (STAMPS), a fully automatic PS-InSAR processing tool developed by the research group of the first author. The processing time is reduced tremendously with the parallelized processing scheme proposed in this paper compared to the tools currently available in the market. The main advantage of this work is that it can be run on a standard HPC cluster. One limitation is the work is done developed in CRISP; the framework also provides interface in browser to visualize the raw deformation time series and ground displacement rate maps. The algorithm is currently executable in HPC, the code will be released soon after receiving of grant advances over usage since in South-east Asia.

Keywords: Persistent Scatterer, Persistent Scatterer Interferometry, SNAP, STAMPS, High Performance Computing

I. INTRODUCTION

Lunched by the European Union's Copernicus program, the Sentinel-1 constellation captures earth-occult S01 data with high revisit frequency and wide coverage. Accelarated since 2014, the related Earth Observation of Sentinel-1 time series are now available for the public via the PS-InSAR processing tool developed by the research group of the first author [1]. By using open source and cross-platform, the toolchain composed of SNAP [6], SNAPS/STAMPS [7] and STAMPS [8, 9] serves as a core for the semi-automated PS-InSAR processing. Sentinel-1 data are usually processed by the researchers separately due to the lack of a fully automated PS-InSAR processing system.

As the data input of the workflow [6], sets of Sentinel-1 correlation captures are converted to S01 data with high revisit frequency and wide coverage. Accelarated since 2014, the related Earth Observation of Sentinel-1 time series are now available for the public via the PS-InSAR processing tool developed by the research group of the first author [1]. By using open source and cross-platform, the toolchain composed of SNAP [6], SNAPS/STAMPS [7] and STAMPS [8, 9] serves as a core for the semi-automated PS-InSAR processing. Sentinel-1 data are usually processed by the researchers separately due to the lack of a fully automated PS-InSAR processing system.

In this work, we propose a fully automated PS-InSAR framework using the SNAP [6] data with open source open source software packages, including SNAPS and STAMPS. To utilize the parallel computational power of HPC, the admissible parallel processing scheme is proposed. The parallel processing tasks, which are independent of each other and reusable in distributed clusters. Due to the acceleration of HPC, the end-to-end processing time can be reduced from several days down to 6 hours. Meanwhile, a user-friendly web interface

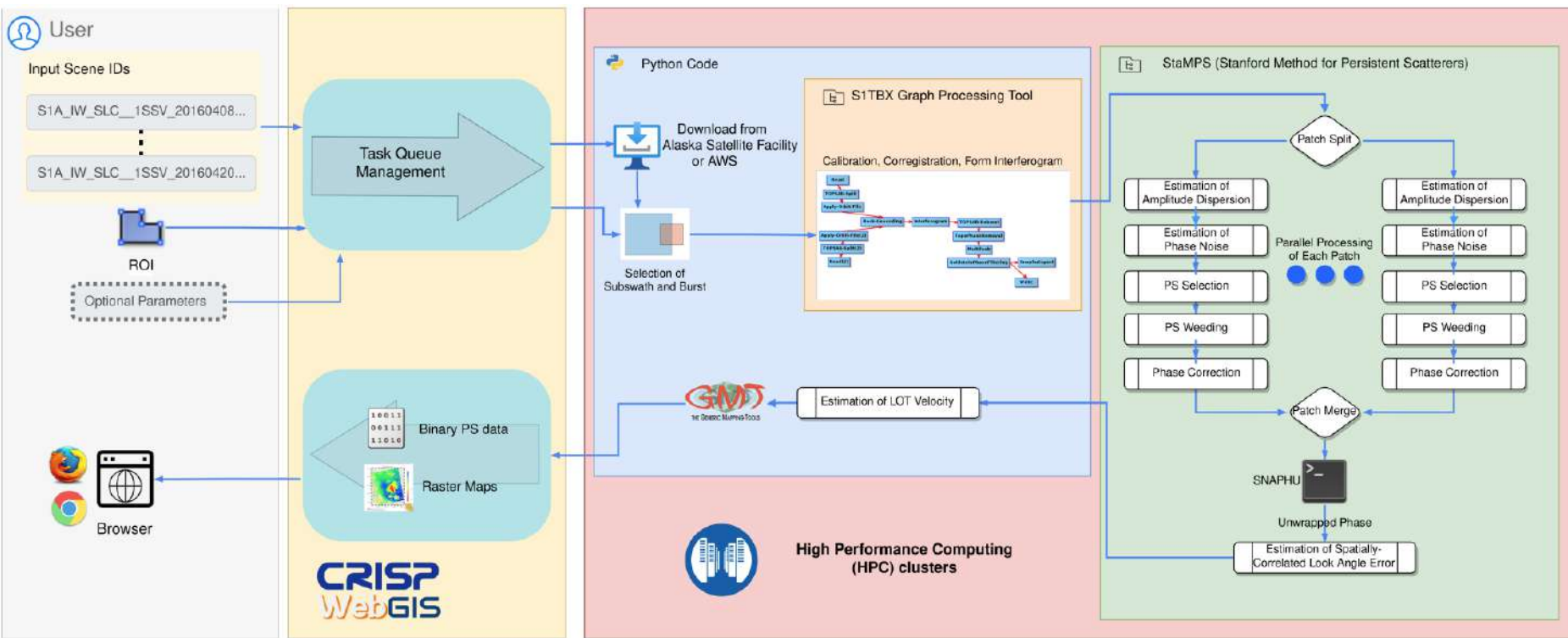
978-1-6654-2702-0/22/\$31.00 ©2022 IEEE

927

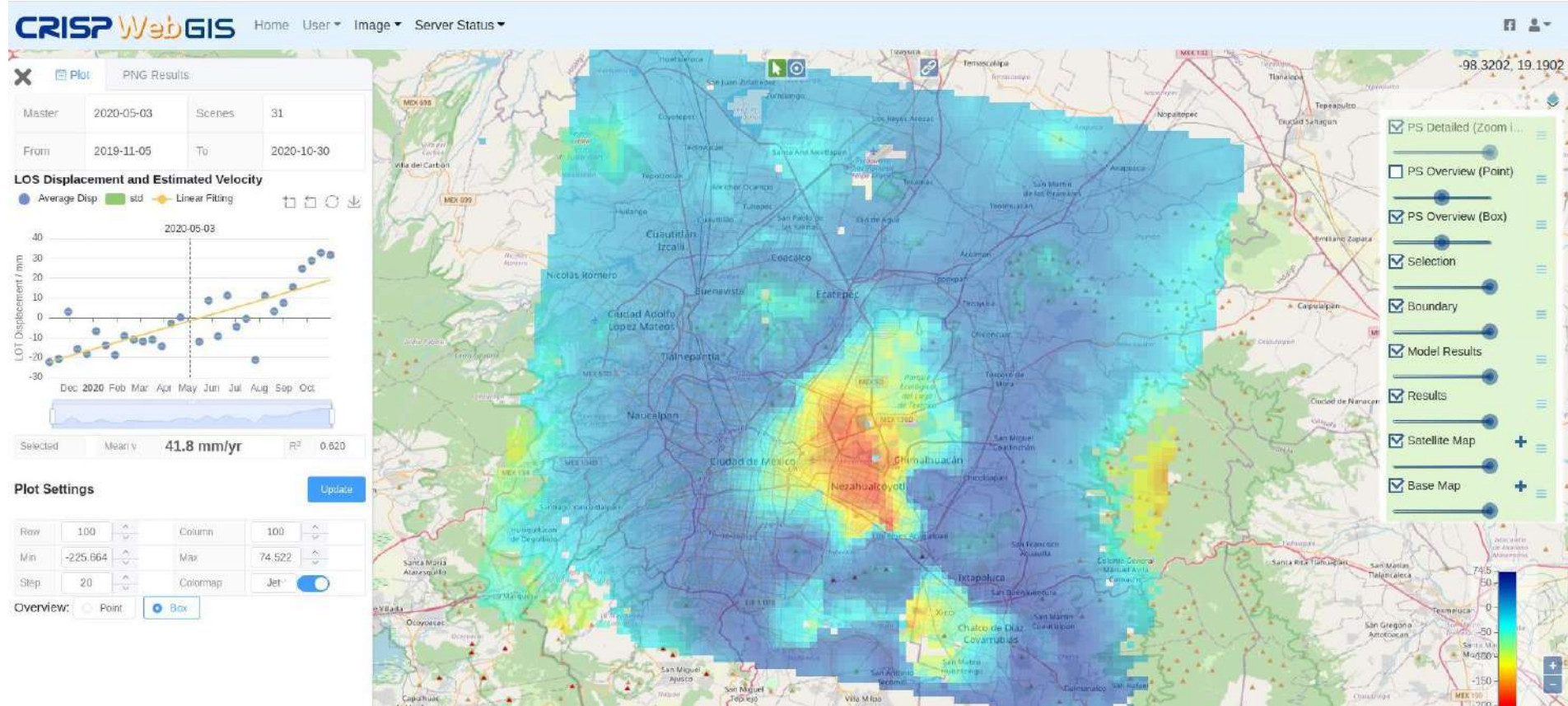
IGARSS 2022

PS-InSAR for Ground Deformation Monitoring

- Existing PS-InSAR processing often requires **manual inputs** within workflow and is always **slow**. Moreover, all single-look complex data **must be downloaded**
- Processing time reduces to ~ 6 hours (versus few-day requirement)

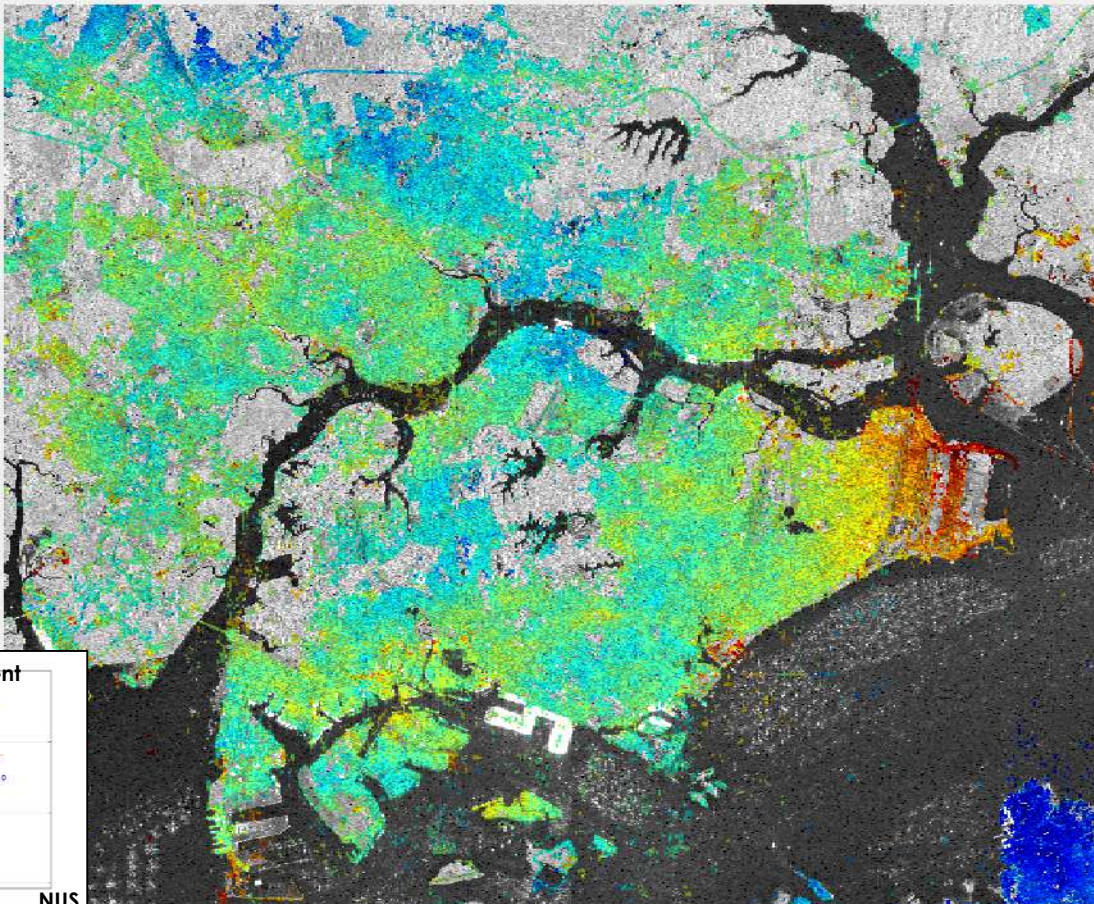


Interactive Visualisation at CRISP Web GIS



PS-InSAR Processing of Sentinel-1 over Singapore

Line-of-Sight Velocity



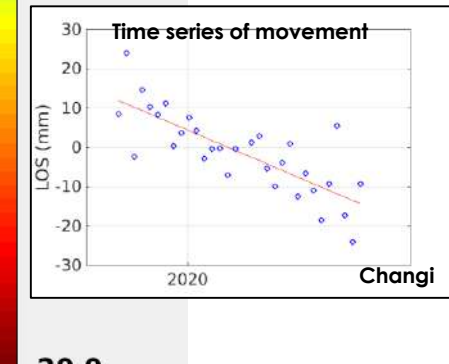
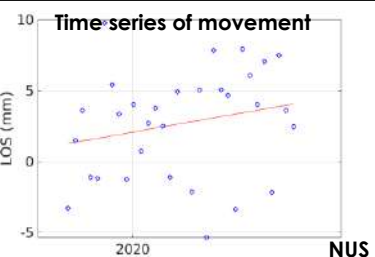
24.8

16th Sept 2020 → 23rd Sept 2021

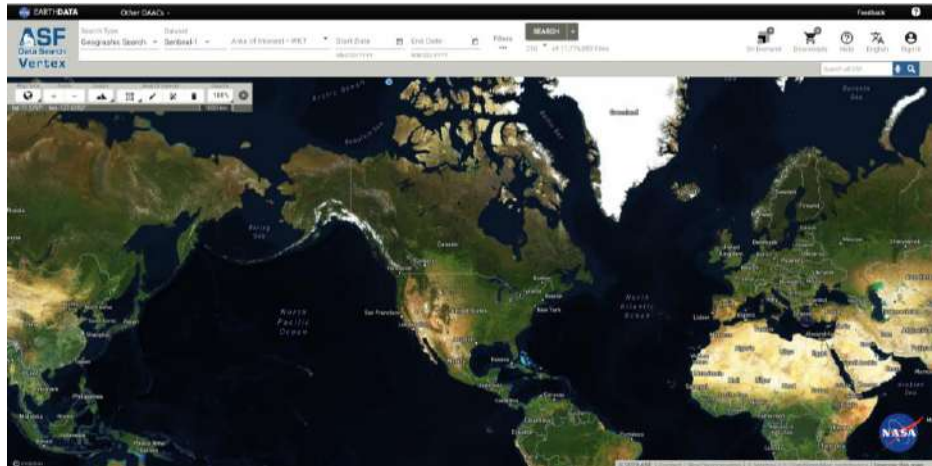
Master scene: 27th Mar 2021

32 single-look complex data,
acquired with interferometric
wide swath mode and in
descending orbit

mm/yr



Freely Available SAR Remotely Sensed Data



Alaska Satellite Facility – Vertex

<https://search.asf.alaska.edu/#/>

<https://search.asf.alaska.edu/#/>



Copernicus Open Access Hub
<https://scihub.copernicus.eu/dhus/>

PlanetScope (5th June 2023)



COSMO-SkyMed Second Generation (6th May 2023)



Tengah
Air Base